

# Response to the Comments on the IEEE TVT Manuscript (VT-2025-03546)

Ke Wang, Chan-Tong Lam, Benjamin K. Ng, and Yue Liu

November 3, 2025

## To AE

---

**Comment:** While this manuscript presents valuable theoretical contributions to near-field RIS systems, the reviewers identify several major issues that must be addressed before further consideration. The contribution of this manuscript should be clarified through a more explicit comparison with prior works. The realism of the modeling assumptions requires stronger justification, particularly regarding the rigor of approximations across diverse scenarios. In addition, important technical details are missing, including clearer terminology, fuller derivations, and deeper integration and discussion of theoretical results. Finally, the limited discussion of practical applicability to IRS-assisted systems and the lack of experimental considerations further weaken the current manuscript.

**Response:** We sincerely thank the editor for the valuable comments. We have thoroughly revised the manuscript to address concerns regarding contribution clarification, modeling rationality, and technical completeness. In the revised manuscript, we have replaced "power loss (PL)" with "remaining power (RP)" (i.e.,  $RP = 1 - PL$ ) to better describe the power that remains after a signal passes through an RIS pixel.

Regarding the contribution, the introduction and Table I provide a systematic comparison with existing studies (Cases I and II in Table I), clearly identifying that this work is the first to analyze the coupling between phase-dependent amplitude (PDA) and phase shift error (PSE), and to introduce two novel reflection models (Cases III and IV in Table I) that consistently capture hardware non-idealities.

To improve rigor, we have added detailed derivations of the approximated PDA model with error terms, demonstrating that the reflected power converges consistently with theoretical results. Moreover, the proposed unified analytical framework and the polynomial upper bounds derived from Taylor expansion show excellent agreement with Monte Carlo simulations, thus validating the accuracy and generality of the approximations.

Finally, we refined the derivations of the near-field channel and spectral efficiency bounds and verified their practical applicability under multiple scenarios. Overall, these revisions have greatly improved the paper's technical soundness and practical relevance. We believe that all of the concerns have been properly addressed.

## To Reviewer 1

---

**Comment 1.1:** The Cases I-IV proposed in the manuscript do cover some typical scenarios, but the assumptions are overly idealized. In particular, Cases III and IV assume that the phase errors of PSE and PDA are either completely consistent or completely independent, which are hardly achievable in practical hardware. A more common scenario is that there exists a certain degree of correlation rather than such extreme assumptions. If this intermediate scenario is neglected, the practicality of the model may be limited. It is suggested to introduce a correlation coefficient parameter in the theoretical part, or verify the impact of different correlations on performance through sensitivity analysis.

**Response 1.1:** We sincerely thank the reviewer for this valuable comment. Indeed, assuming that the PEs in the PSE and PDA are either completely consistent or entirely independent and identically distributed (i.i.d.) represents an idealized scenario. To bridge this gap and better reflect practical hardware behavior, we introduce a correlation coefficient, denoted by  $\iota$ , to quantify the correlation level between the PEs in the PDA and those in the PSE. Specifically, the motivation is that differential degradation of RIS components (e.g., varactor diodes) desynchronizes the errors of the PSE and PDA, thereby increasing their statistical independence. Consequently, as the RIS behavior increasingly approximates an i.i.d. noise model, the correlation coefficient  $\iota$  decreases toward 0, reflecting more random and decoupled uncertainties caused by hardware degradation.

To formalize this relationship, consider the total power emitted from the RIS:

$$P_{\text{RIS}} = \left| \sum_{m=1}^M \sqrt{P_{\text{AP} \rightarrow m}} \beta(\phi_m + \bar{\Delta}_m) \exp(-j(\phi_m + \Delta_m)) \right|^2,$$

where  $\Delta_m$  and  $\bar{\Delta}_m$  are random variables (RVs). We model their dependence by defining  $\bar{\Delta}_m = \iota \Delta_m + \sqrt{1 - \iota^2} \check{\Delta}_m$ , where  $\check{\Delta}_m$  denotes an extra RV that is i.i.d. with  $\Delta_m$ . By construction, the coefficient  $\iota \in [0, 1]$  characterizes the correlation between the PE in the PDA (i.e.,  $\bar{\Delta}_m$ ) and in the PSE (i.e.,  $\Delta_m$ ): when  $\iota = 0$ ,  $\Delta_m$  and  $\bar{\Delta}_m$  are i.i.d.; when  $\iota = 1$ , they are identical; and for intermediate values  $\iota \in (0, 1)$ , they exhibit partial correlation.

Importantly, we reveal that the impact of  $\iota$  on system performance depends on the operating region of the RIS phase shifts. In particular, as the RIS phase shifts approach the ends of their range, the RP under i.i.d. PEs (i.e.,  $\iota = 0$ ) becomes smaller than that under identical PEs (i.e.,  $\iota = 1$ ); however, this relationship reverses near the middle of their range. Therefore, when the RIS is new and its components are highly correlated ( $\iota = 1$ ), the phase shift set  $\{\phi_m\}_{m=1}^M$  should be configured near the ends of the range to achieve a higher  $\Gamma$ . In contrast, after long-term use with reduced correlation ( $\iota = 0$ ),  $\{\phi_m\}_{m=1}^M$  should be set close to the middle of the range. We provide theoretical analyses and simulation results in the revised manuscript. **The revised portion is shown below.**

### (Page 2) Sec. I, B

...Thus, from a practical perspective, the PDA may also exist the PE. To this end, in this paper, we consider three regimes: (i) perfect transfer of the PE from the PSE to the PDA, i.e.,  $\iota = 1$  in Cases III and IV in Table I; (ii) fully random pixel imperfections that induce i.i.d. noise at the PDA, i.e.,  $\iota = 0$  in Cases III and IV in Table I; and (iii) intermediate correlation levels with  $\iota \in (0, 1)$ . In practice, the pixel hardware failure [14-17] progressively shifts the system from (i) toward (ii). Specifically, differential degradation of RIS components (e.g., varactor diodes) desynchronizes the errors between the PSE and the PDA, thereby increasing their *statistical independence*. Consequently, as the RIS behavior approaches an i.i.d. noise model, the correlation coefficient  $\iota$  decreases over time and approaches 0, reflecting the emergence of random, decoupled uncertainties driven by hardware degradations [17]...

### (Pages 4) Sec. III

...Suppose there is an RIS with  $M$  pixels and each transceiver is equipped with a single isotropic antenna. The total power that is emitted from the RIS can be obtained as  $P_{\text{RIS}} = \left| \sum_{m=1}^M \sqrt{P_{\text{AP} \rightarrow m}} \beta(\phi_m + \bar{\Delta}_m) \exp(-j(\phi_m + \Delta_m)) \right|^2$ , where  $\Delta_m$ ,  $\bar{\Delta}_m$ , and  $\check{\Delta}_m$  are RVs. Note that  $\bar{\Delta}_m = \iota \Delta_m + \sqrt{1 - \iota^2} \check{\Delta}_m$  and  $\check{\Delta}_m$  is i.i.d. with  $\Delta_m$ . The coefficient  $\iota \in [0, 1]$  is introduced to characterize the correlation between the PE in the PDA (i.e.,  $\bar{\Delta}_m$ ) and in the PSE (i.e.,  $\Delta_m$ ). When  $\iota = 0$ ,  $\Delta_m$  and  $\bar{\Delta}_m$  are i.i.d., if  $\iota = 1$ ,  $\Delta_m = \bar{\Delta}_m$ . For intermediate values  $\iota \in (0, 1)$ ,  $\Delta_m$  and  $\bar{\Delta}_m$  exhibit partial correlation...

### (Pages 5) Sec. III

...To model the quantization errors and hardware degradations of the RIS, we assume that the PEs  $\delta_m$  and  $\bar{\delta}_m$  at the  $m$ -th pixel follow a  $\mathcal{UF}$  distribution [10], i.e.,  $\delta_m$  and  $\bar{\delta}_m \sim \mathcal{UF}[-\tau, \tau]$ , where  $\tau \in [0, \pi/2]$ . The

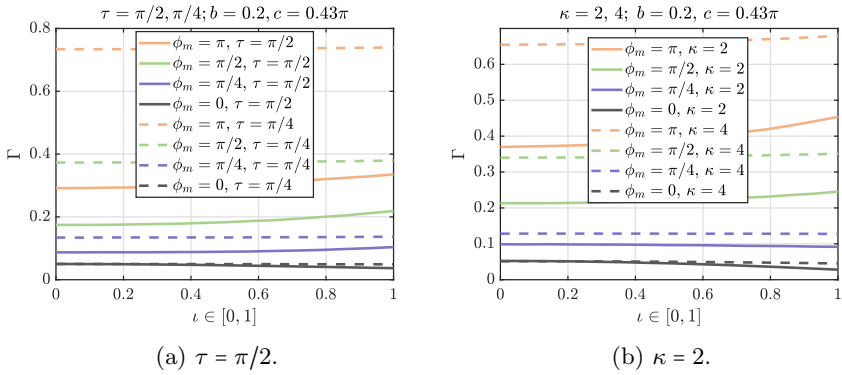


Figure 2:  $\iota$  vs.  $\Gamma$  considering  $\mathcal{UF}$  and  $\mathcal{VM}$  RVs.

corresponding probability density function (PDF) is  $f_{\mathcal{UF}}(\delta) = \frac{1}{2\tau}$  where  $\delta \in [-\tau, \tau]$  or is zero otherwise. Hence, the reflection coefficient is  $\beta(\phi_m + \bar{\delta}_m) \exp(-j(\phi_m + \delta_m))$ , where  $\bar{\delta}_m = \iota \delta_m + \sqrt{1 - \iota^2} \check{\delta}_m$ ,  $\iota \in [0, 1]$  and  $\check{\delta}_m$  is i.i.d. with  $\delta_m$ . For imperfect channel estimations of the RIS, we assume that the errors  $\gamma_m$  and  $\bar{\gamma}_m$  in the  $m$ -th pixel follows zero-mean  $\mathcal{VM}$  distributions [31], i.e.,  $\gamma_m$  and  $\bar{\gamma}_m \sim \mathcal{VM}(0, \kappa)$ , where  $\kappa$  is concentration parameter. Accordingly, the PDF is  $f_{\mathcal{VM}}(\gamma) = \frac{\exp(\kappa \cos(\gamma))}{2\pi I_0(\kappa)}$  where  $\gamma \in [-\pi, \pi]$  and  $I_n(\kappa)$  is the modified Bessel function of the first kind of order  $n$  with  $\kappa \geq 1$ . Thus, the reflection coefficient is  $\beta(\phi_m + \bar{\gamma}_m) \exp(-j(\phi_m + \gamma_m))$ , where  $\bar{\gamma}_m = \iota \gamma_m + \sqrt{1 - \iota^2} \check{\gamma}_m$ ,  $\iota \in [0, 1]$  and  $\check{\gamma}_m$  is i.i.d. with  $\gamma_m$ ...

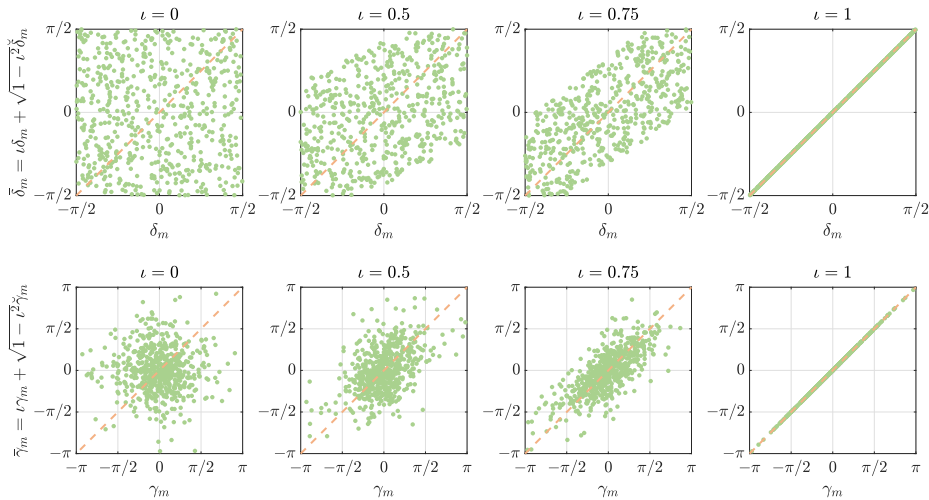


Figure 1: Scatter plots of  $\mathcal{UF}$  and  $\mathcal{VM}$  RVs for different correlation coefficients  $\nu \in [0, 0.5, 0.75, 1]$ .

...The top row of Fig. 1 plots the characteristics of  $\bar{\delta}_m = \iota\delta_m + \sqrt{1-\iota^2}\check{\delta}_m$  when i.i.d. RVs  $\delta$  and  $\check{\delta}_m$  follow a  $\mathcal{UF}$  distribution with  $\tau = \pi/2$ . As the correlation coefficient  $\iota$  increases from 0 to 1, the scatter points transition from occupying a square region to converging along the diagonal, fully aligning at  $\iota = 1$ . In the third figure of this row, the overall trend of the green dots is flatter than the orange line. This is because the best-fit line for the green dots is not the line  $\bar{\delta}_m = \delta_m$ , but rather  $\bar{\delta}_m = 0.75\delta_m$ . The bottom row of Fig. 1 presents the same construction method and i.i.d. RVs  $\gamma$  and  $\check{\gamma}_m$  follow a  $\mathcal{VM}$  distribution. As  $\iota$  increases, the correlation strengthens and points cluster toward the diagonal, yet the central concentration of the  $\mathcal{VM}$  and sparse tails result in higher density at the center...

(Pages 9) Sec. III. C

**...Remark II** (If  $\phi_m$  approaches to 0, why  $\Gamma$  decreases when  $\iota$  increases?): As observed in Figs. 2(a) and 2(b), the RP  $\Gamma$  decreases as  $\phi_m$  approaches 0. For instance,  $\Gamma$  is slightly lower at  $\phi_m \approx 0$  than at  $\phi_m \approx \pi/4$ . This is because when  $\phi_m \approx 0$ , the system operates near the linear region of the phase response function  $\beta(\cdot)$ . As the correlation coefficient  $\iota$  increases from 0 toward 1, the amplitude and phase noise become increasingly coupled. This coupling induces a negative covariance between the amplitude and the phase. We provide a strict proof of  $\Gamma(0)|_{\iota=0} > \Gamma(0)|_{\iota=1}$  in Appendix B. Fig. 3 verify Remark II through

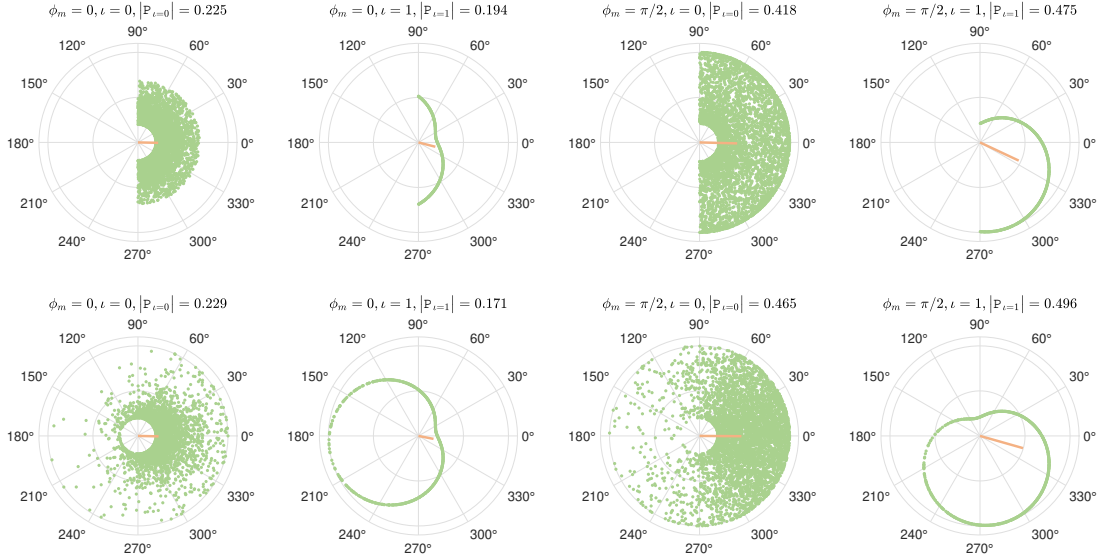


Figure 3: Vector field distribution with  $\mathcal{UF}$  and  $\mathcal{VM}$  RVs to verify Remark II. Note that  $P = P(\bar{\Delta}, \Delta)$  as Appendix B defines.

*Monte Carlo simulations of vector field distributions under  $\mathcal{UF}$  and  $\mathcal{VM}$  RVs, respectively. In particular, when  $\phi_m = 0$ ,  $|P_{i=1}| < |P_{i=0}|$  and the inequality is reversed when  $\phi_m = \pi/2$ ...*

### (Page 9) Sec. III. D

...Figs. 4a and 4b illustrate that as the RIS phase shifts approach the ends of their range, the RP under i.i.d. PEs in both the PSE and PDA cases becomes smaller than that under identical PEs, whereas this relationship reverses when the phase shifts are near the middle of their range. Therefore, when the RIS is new and its components are highly correlated (i.e.,  $\iota = 1$ ), the phase shift set  $\{\phi_m\}_{m=1}^M$  should be configured near the ends of their range to achieve a higher  $\Gamma$ . Conversely, after long-term use with reduced correlation (i.e.,  $\iota = 0$ ),  $\{\phi_m\}_{m=1}^M$  should be set close to the middle of the range...

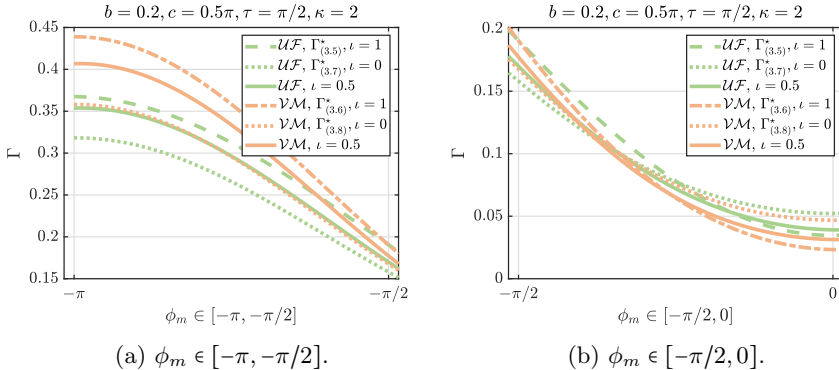


Figure 4: RP comparison under different  $\iota$ .

### (Pages 13, 15) Sec. V. A and D

...illustrates the SE for different  $\iota$ ,  $a$ ,  $b$ , and  $c$ . As expected, when  $\phi_m = \phi_L$ , SE decreases as  $\iota$  increases, consistent with Figs. 4 and 13. Moreover, SE increases with smaller  $a$  and decreases with larger  $b$ . In contrast,  $c$  has negligible impact on SE because it only shifts the PDA curve...

...show the feasible sets in the complex plane and their corresponding areas for the different propositions in Sec. III. As expected, greater uncertainties lead to smaller feasible set areas...

---

**Comment 1.2:** In Proposition 3.5, the upper bound of power loss is approximated using a first-order Taylor expansion. However, as shown in Fig. 7(a), when the phase error is close to  $\pi/2$ , there is a significant discrepancy between the analytical results and Monte Carlo simulations. In Remark 8, the authors only mention that "the approximate expression utilizes the Taylor expansion around  $x = 0$ , which may be somewhat inaccurate when  $x = \pi/2$ " but fail to further quantify the range of such discrepancies

(e.g., maximum error value, deviation rate with respect to  $x$ ) or explicitly clarify the acceptable range of  $x$  for this approximation. It is recommended to supplement the error upper bound analysis, quantify the applicable boundaries of the current approximation, and verify the robustness of its derivation under non-ideal conditions, which is necessary to enhance the rigor of the theoretical analysis.

**Response 1.2:** We sincerely thank the reviewer for this valuable comment. We agree that when the phase error is close to  $\pi/2$ , there exists a significant discrepancy between the AN and the MC results. The mismatch is caused by insufficient expansion terms. We have fixed this issue, and the AN and MC results now match well. In addition, we have added and plotted the corresponding error terms in Props. 3.1–3.10 of Sec. III. **The revised portion is shown below.**

### (Page 5) Sec. III, A

**Proposition 3.1** ( $\beta \exp(-j\delta_m)$ , the PDA is a constant and the PSE contains **UF noises**): *When the  $m$ -th PDA is a constant  $\beta$ , and the PSE includes  $\delta_m \sim \mathcal{UF}[-\tau, \tau]$  where  $\tau \in [0, \pi/2]$ , then the RP  $\Gamma$  in (9) can be obtained as*

$$\Gamma_{(3.1)} = |\mathbb{E}\{\beta \exp(-j\delta_m)\}|^2 = \beta^2 \left(1 - \frac{1}{3}\tau^2 + \frac{2}{45}\tau^4 - \frac{1}{360}\tau^6 + \frac{1}{14400}\tau^8\right) + \mathcal{O}(\tau^{10}), \quad (1)$$

where  $\mathcal{O}(\cdot)$  denotes higher-order terms.

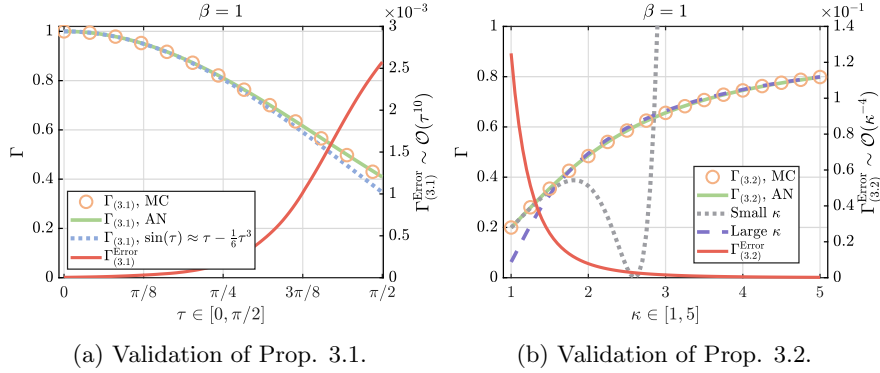


Figure 5: Validation of Case I.

...Fig. 5a reveals that  $\Gamma_{(3.1)}$  needs at least the first three terms of the Taylor series expansion of  $\sin(\tau)$ . The error term is  $\Gamma_{(3.1)}^{\text{Error}} = |\Gamma_{(3.1)}^{\text{MC}} - \Gamma_{(3.1)}^{\text{AN}}| \sim \mathcal{O}(\tau^{10})$  and becomes significant when  $\tau$  approaches  $\pi/2$ ....

### (Pages 6-10) Sec. III, A, B, C, and D

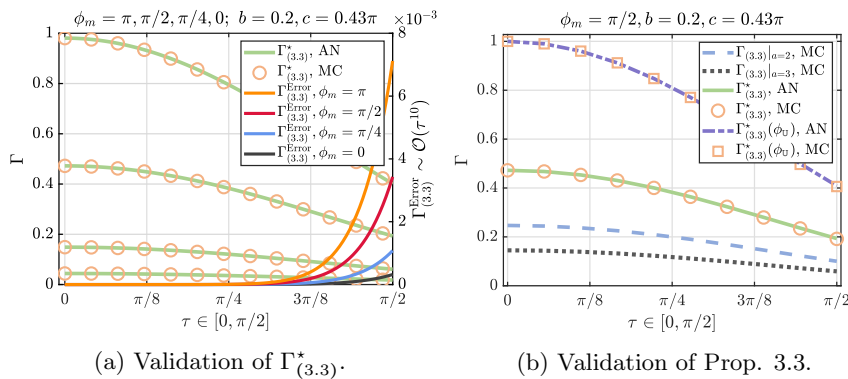


Figure 6: Validation of Prop. 3.3.

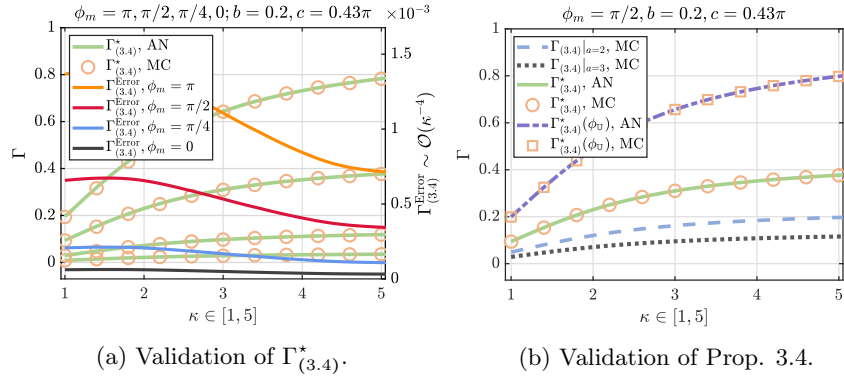


Figure 7: Validation of Prop. 3.4.

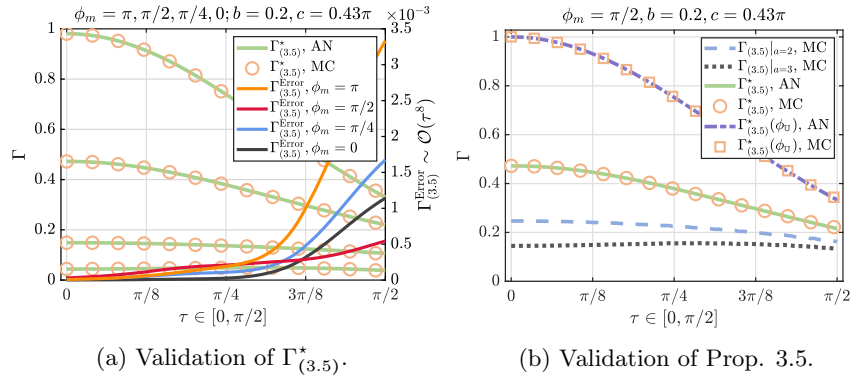


Figure 8: Validation of Prop. 3.5.

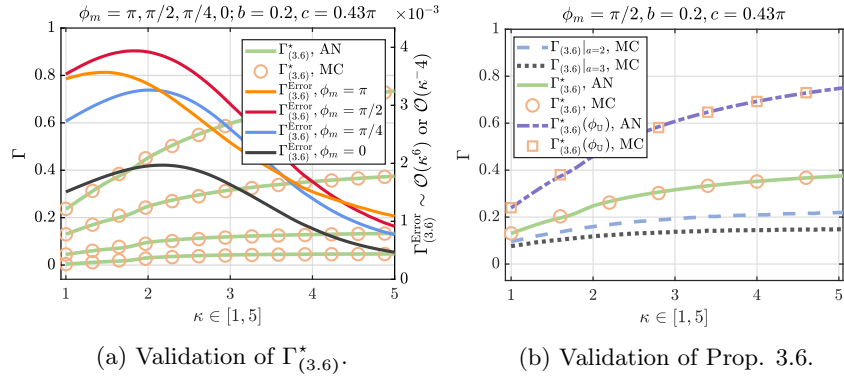


Figure 9: Validation of Prop. 3.6.

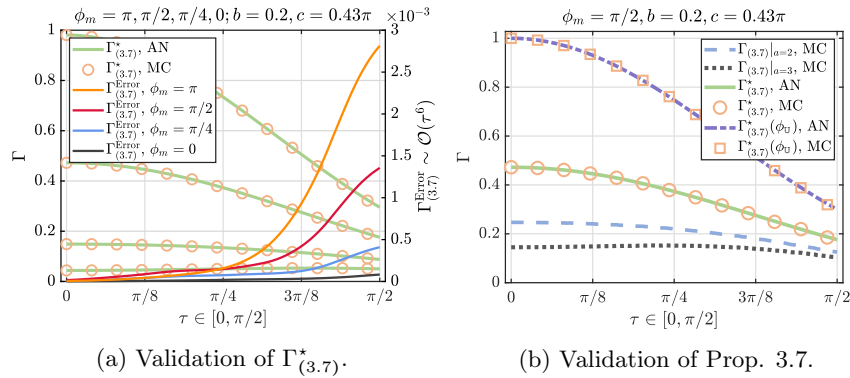


Figure 10: Validation of Prop. 3.7.

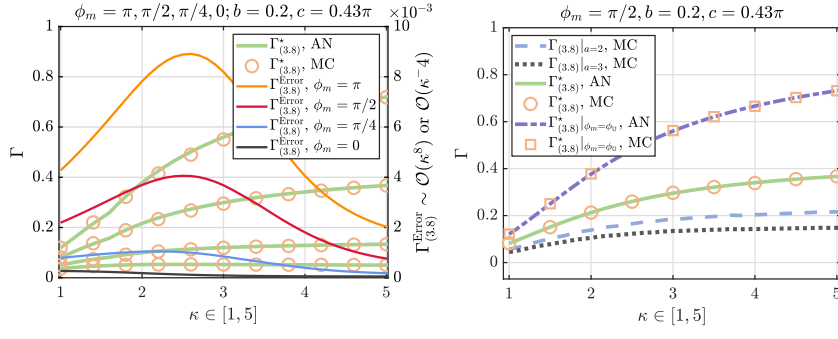


Figure 11: Validation of Prop. 3.8.

(a) Validation of  $\Gamma_{(3.8)}^*$ . (b) Validation of Prop. 3.8.

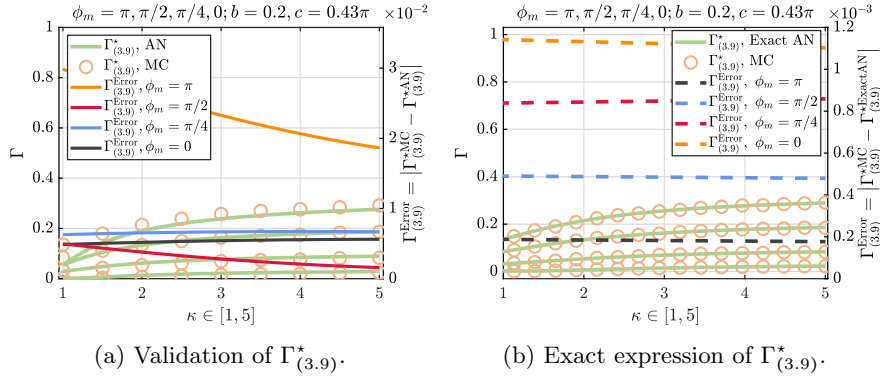


Figure 12: Validation of Prop. 3.9.

(a) Validation of  $\Gamma_{(3.9)}^*$ . (b) Exact expression of  $\Gamma_{(3.9)}^*$ .

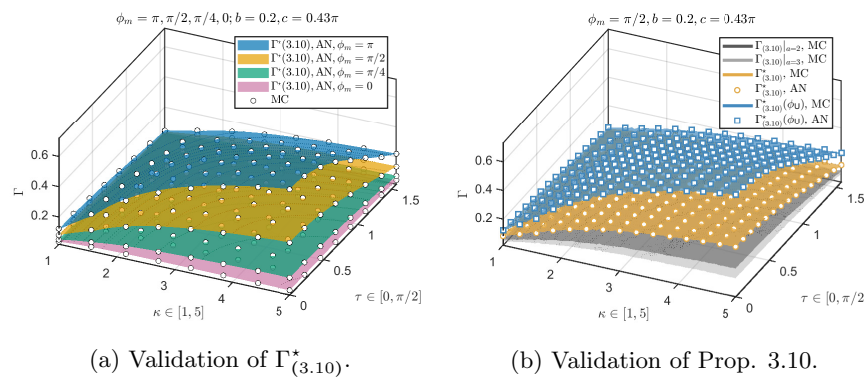


Figure 13: Validation of Prop. 3.10.

---

**Comment 1.3:** In Remark 14, it is proposed that when the number of pixels is sufficiently large, the power loss  $\Gamma_m$  of each pixel can be assumed to be approximately equal, and this assumption is used in deriving the SE upper and lower bounds. However, the physical rationality of this assumption has not been fully elaborated: in near-field scenarios, distance differences between different pixels and the AP/user are significant, and the fading characteristics and phase shifts of cascaded channels vary, which will inevitably lead to individual differences in  $\Gamma_m$ . Moreover, such differences may be amplified in the near field. Currently, the authors only generally state that "the validity of the approximation is verified" through simulations in Section V, but do not specifically demonstrate the distribution characteristics of  $\Gamma_m$  across different pixels or quantify the impact of this assumption on the SE derivation results. It is suggested to derive the error upper bound for approximating  $\Gamma_m$  as a constant theoretically, to clarify the applicable conditions of this assumption (e.g., the number of pixels must satisfy  $M \geq a$  certain threshold); otherwise, the reliability of the SE upper and lower bounds may be compromised.

**Response 1.3:** We sincerely thank the reviewer for this valuable comment. Indeed, we totally agree that in near-field scenarios, the differences in distances, fading characteristics, and phase shifts among pixels may lead to noticeable variations in  $\Gamma_m$ , which could affect the validity of assuming equal RP across pixels. By leveraging the extended Glivenko–Cantelli theorem, we rigorously prove the asymptotic convergence of the RP to its theoretical value, thereby establishing the statistical foundation for subsequent analysis. Specifically, the extended theorem states that if the empirical distribution function of a deterministic sequence converges weakly to a probability distribution function, then the average of any continuous and bounded function over that sequence converges to the expectation of the corresponding random variable. Consequently, when the number of pixels is sufficiently large, we can assume that the phase  $\phi_m$  is uniformly distributed over  $[-\pi - c, \pi + c]$ .

Based on this result, we observe that when  $\iota = 0$ , as  $M$  increases from 1 to 200, the Monte Carlo (MC) result

$$\Gamma_M = \left| \frac{1}{M} \sum_{m=1}^M \beta(\phi_m + \bar{\Delta}_m) \exp(-j\Delta_m) \right|^2$$

converges asymptotically to the analytical (AN) limit

$$\Gamma_\infty = \left| \mathbb{E} \{ \beta(\phi + \bar{\Delta}) \exp(-j\Delta) \} \right|^2.$$

In contrast, when  $\iota = 1$ , a larger  $M$  (e.g.,  $M = 500$ ) is required to achieve similar convergence due to stronger correlation between phase errors. **The revised portion is shown below.**

### (Pages 4 and 5) Sec. III

...Therefore, assuming that the noise RVs on different pixels (e.g.,  $m = 1, 2$ ) are i.i.d.,  $P_{\text{RIS}}$  can be rewritten as

$$\begin{aligned} P_{\text{RIS}} &= \left| \sum_{m=1}^M \sqrt{P_{\text{AP} \rightarrow m}} \underbrace{\beta(\phi_m + \bar{\Delta}_m)}_{\text{PE}} \underbrace{\exp(-j\Delta_m)}_{\text{PE}} \right|^2 \\ &\stackrel{(i)}{=} P_{\text{AP} \rightarrow 1} \left| \sum_{m=1}^M \beta(\phi_m + \bar{\Delta}_m) \exp(-j\Delta_m) \right|^2 \\ &= M^2 P_{\text{AP} \rightarrow 1} \left| \frac{1}{M} \sum_{m=1}^M \beta(\phi_m + \bar{\Delta}_m) \exp(-j\Delta_m) \right|^2 \\ &\xrightarrow{M \rightarrow \infty} M^2 P_{\text{AP} \rightarrow 1} \underbrace{\left| \mathbb{E} \{ \beta(\phi + \bar{\Delta}) \exp(-j\Delta) \} \right|^2}_{\substack{\text{Square Law} \\ \text{Remaining Power } \Gamma \in (0,1)}}, \end{aligned} \quad (2)$$

where (i) is obtained when the pixels are all with the same transmit power  $P_{\text{AP} \rightarrow 1} = P_{\text{AP} \rightarrow 2} = \dots = P_{\text{AP} \rightarrow M}$ , respectively. As the number of reflecting elements  $M$  becomes sufficiently large, the phase shift set  $\{\phi_m\}_{m=1}^M$ , which is designed to be densely and uniformly distributed over the interval  $[-\pi/2 - c, \pi/2 + c]$ , form a sequence whose empirical distribution function converges to that of a continuous  $\mathcal{UF}$  distribution over  $[-\pi/2 - c, \pi/2 + c]$ . By considering an extension of the *Glivenko–Cantelli theorem* [30], for the bounded continuous functions  $\beta(\phi + \bar{\Delta}) \exp(-j\Delta)$ , the final step of (3) is obtained...

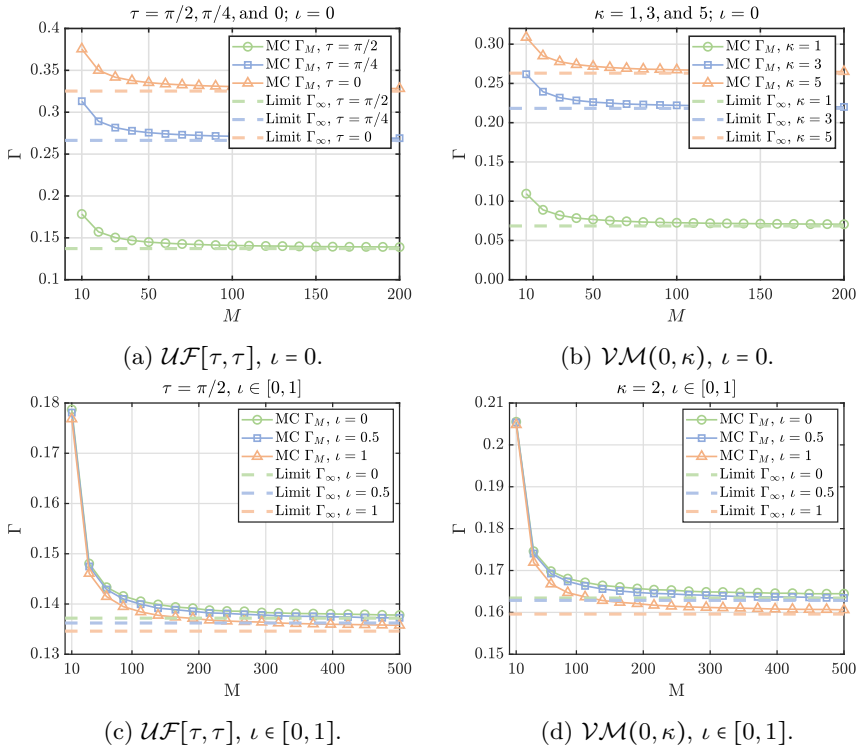


Figure 14: Validation of (8),  $\iota = 0$  or 1.

...It can be observed from Figs. 14a and 14b that, when  $\iota = 0$ , as  $M$  increases from 1 to 200, Monte Carlo (MC) result  $\Gamma_M = \left| \frac{1}{M} \sum_{m=1}^M \beta(\phi_m + \bar{\Delta}_m) \exp(-\jmath\Delta_m) \right|^2$  converges asymptotically to AN limit  $\Gamma_\infty = |\mathbb{E}\{\beta(\phi + \bar{\Delta}) \exp(-\jmath\Delta)\}|^2$ . Besides, as the PE becomes more severe (i.e.,  $\tau$  increases from 0 to  $\pi/2$  and  $\kappa$  increases from 1 to 5),  $\Gamma_M$  and  $\Gamma_\infty$  decrease accordingly. Besides, from Figs. 14c and 14d, if  $\iota = 1$ , the same convergence behavior is observed, i.e., as  $M$  grows, the MC result  $\Gamma_M$  approaches its AN limit  $\Gamma_\infty$ . More importantly, both  $\Gamma_M$  and  $\Gamma_\infty$  with  $\iota = 1$  are smaller than these with  $\iota = 0$ . This implies if an RIS has a sufficiently large number of elements (e.g.,  $M > 200$ ) and the average phase approaches zero, then fully coupled noise (i.e.,  $\iota = 1$ ) is more detrimental than i.i.d. noise (i.e.,  $\iota = 0$ ). The top row of Fig. 1 plots the characteristics of  $\bar{\delta}_m = \iota\delta_m + \sqrt{1 - \iota^2}\check{\delta}_m$  when i.i.d. RVs  $\delta$  and  $\check{\delta}_m$  follow a  $\mathcal{UF}$  distribution with  $\tau = \pi/2$ . As the correlation coefficient  $\iota$  increases from 0 to 1, the scatter points transition from occupying a square region to converging along the diagonal, fully aligning at  $\iota = 1$ . In the third figure of this row, the overall trend of the green dots is flatter than the orange line. This is because the best-fit line for the green dots is not the line  $\bar{\delta}_m = \delta_m$ , but rather  $\bar{\delta}_m = 0.75\delta_m$ . The bottom row of Fig. 1 presents the same construction method and i.i.d. RVs  $\gamma$  and  $\check{\gamma}_m$  follow a  $\mathcal{VM}$  distribution. As  $\iota$  increases, the correlation strengthens and points cluster toward the diagonal, yet the central concentration of the  $\mathcal{VM}$  and sparse tails result in higher density at the center...

---

**Comment 1.4:** *The manuscript claims to be the first to analyze the coupling effect between PSE and PDA, but the contributions and boundaries with existing work remain unclear in the current presentation. Secondly, the settings in Cases III/IV—where phase errors (PE) in PSE and PDA are “completely consistent” or “independent and identically distributed”—fail to clarify how these proposed settings advance beyond the single modeling of PDA in [19], [20]. Additionally, in terms of error propagation analysis, how the derived upper bound of power loss quantifies the impact of coupling errors on performance has not been compared with existing work in a targeted manner. It is recommended to supplement such targeted comparisons.*

**Response 1.4:** We sincerely thank the reviewer for this valuable comment. We agree that the distinctions between our work and existing studies, as well as the specific contribution boundaries, were not sufficiently clarified in the original manuscript. To address this concern, we have clarified the differences between this work and prior studies in Table 1. Specifically, references [19] and [20] correspond to Case II, which is captured by Props 3.3 and 3.4 in our framework. In contrast, we introduce the correlation coefficient  $\iota \in [0, 1]$  to characterize the continuum between “completely consistent” PEs ( $\iota = 1$ ) and “independent and identically distributed” PEs ( $\iota = 0$ ), i.e., Cases III and IV. Moreover, Cases I and II

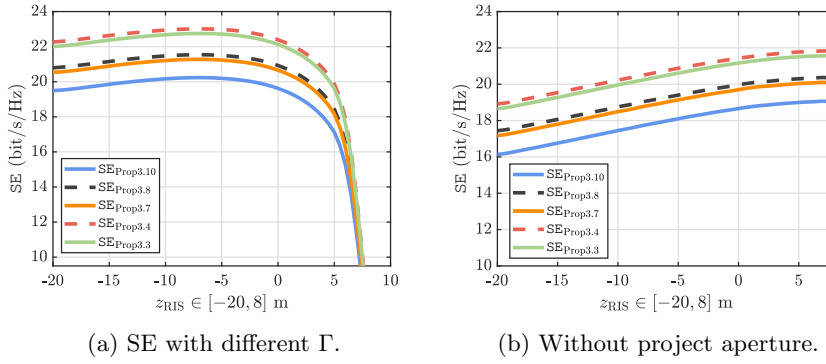
serve as the benchmarks. Accordingly, we not only compare the RP ( $\Gamma$ ) and SE performance between the benchmarks and our proposed models (Cases III and IV), but also compare the designed feasible phase shift set areas, which further highlights the distinction between our coupling-aware model and existing single-error models. **The revised portion is shown below.**

(Page 2) Sec. I

Model	Works	Reflection Coefficient Description	Approximated Model
Perfect	[3-9], [26-28]	...	$1 \cdot \exp(-j\phi)$
Case I	[10-16], [29]	...	$\beta \cdot \exp(-j\Delta)$
Case II	[17-20]	...	$\beta(\phi) \cdot \exp(-j\Delta)$
Case III	This paper	...	$\beta(\phi + \bar{\Delta}) \cdot \exp(-j\Delta)$
Case IV	This paper	...	$\beta(\phi + \bar{\Delta} + \bar{\Theta}) \cdot \exp(-j(\Delta + \Theta))$

Table 1: Comparison between this paper and its related works. Note  $\beta(\cdot) \in (0, 1]$  and  $\phi$  is the designed pixel phase shift.  $\Delta, \bar{\Delta}, \Theta$  and  $\bar{\Theta}$  all denote PE RVs,  $\bar{\Delta} = \iota\Delta + \sqrt{1 - \iota^2}\bar{\Delta}$ , where  $\iota \in [0, 1]$  and  $\bar{\Delta}$  is i.i.d. with  $\Delta$ .  $\Theta$  and  $\bar{\Theta}$  are defined analogously.

(Page 14) Sec. V, C



(a) SE with different  $\Gamma$ . (b) Without project aperture.

Figure 15: System performance for the RIS  $z$ -axis movement.

...Next, we consider the RIS center is set to  $[0, 10, z_{\text{RIS}}]^T$  m with  $z_{\text{RIS}} \in [-20, 10]$  m, and the Doppler effect is neglected. Fig. 23a illustrates that as  $z_{\text{RIS}}$  increases, the SE first rises due to the reduced propagation distance, but then falls as the projected aperture diminishes to nearly zero. However, as shown in Fig. 23b, without the projected aperture, the SE is simply inversely proportional to the distance between the transmitter and receiver. Besides,  $\text{SE}_{\text{Prop.3.10}}$  is smallest, as expected...

(Page 14) Sec. V, D

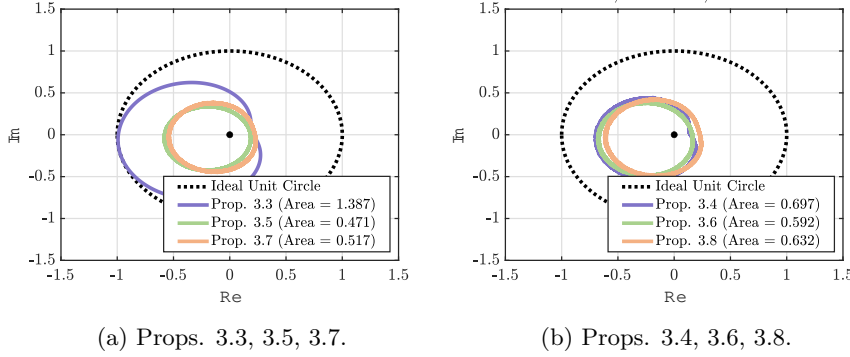
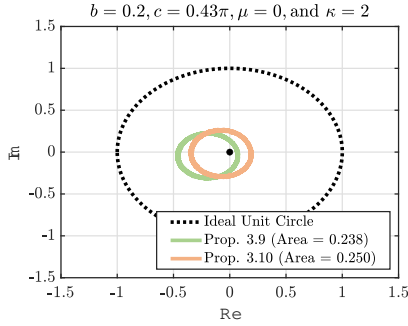
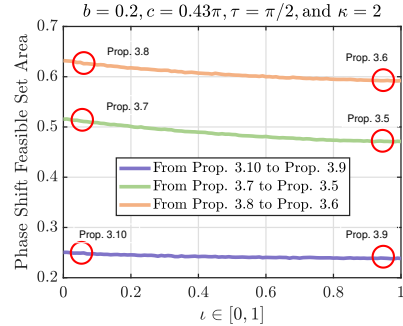


Figure 16: Feasible set and areas.

...Figs. 15 and 16 show the feasible sets for designed RIS phases in the complex plane and their corresponding areas for the different propositions in Sec. III. As expected, greater uncertainties lead to smaller feasible set areas. Moreover, the areas and  $\iota$  are inversely related. This suggests that RIS designs should be optimized to minimize noise coupling, especially during the initial deployment of an RIS...



(a) Props. 3.9 and 3.10.



(b) Feasible set areas vs.  $\iota$ .

Figure 17: Feasible set and areas.

**Comment 1.5:** The design of simulation validation has certain limitations. First, in the analysis of power loss performance (e.g., Figs. 3, 7, 8), parameters  $b = 0.2$  and  $c = 0.43\pi$  are fixed, without exploring the impact of other parameter combinations. For instance, when  $b$  approaches 1 (close to ideal total reflection) or  $b = 0$  (close to complete absorption), the effect of phase error on power loss may change; meanwhile,  $c$ , as the horizontal offset parameter of the PDA model, can take different values that alter the correlation between phase shift and amplitude. Relying solely on simulation results with a single parameter combination is insufficient to support the universality of the conclusions. Second, in Scenario II, the RIS is only considered to move along a straight line "from near the AP to near the user," but it remains unshown whether the impact of distance differences in near-field channels on power loss  $\Gamma_m$  aligns with current conclusions when the RIS moves laterally (perpendicular to the AP-user link) or at non-uniform speeds. The lack of validation for different movement modes may restrict the conclusions to specific scenarios. It is suggested to supplement simulations with multiple parameter combinations to compare the variation trends of power loss under different parameters; meanwhile, to add tests on scenarios such as lateral movement and arc-shaped trajectories of the RIS, thereby verifying the stability of conclusions across diverse scenarios and enhancing the persuasiveness of the argument.

**Response 1.5:** We sincerely thank the reviewer for this valuable comment. Indeed, we agree that the simulation validation in the original version was somewhat limited in scope and did not fully explore the influence of different parameter combinations or movement patterns. In the revised manuscript, we have already added more simulations to verify our results. Specifically, the simulation section has been reorganized into four parts. First, we consider a fixed RIS configuration to validate the analytical results, showing that MC simulations closely match the theoretical expressions of RP and SE under different coupling conditions. Second, we examine the movement of the RIS along the  $x$ -axis, thereby illustrating how horizontal displacement influences the coupling effect and overall system performance. Third, we investigate the RIS displacement along the  $z$ -axis, which reveals the impact of vertical position on reflection power and spectral efficiency. Finally, we provide a comparison of feasible-set areas, which further distinguishes the proposed coupling-error model (Cases III and IV) from the baseline models (Cases I and II). Collectively, these additional results comprehensively confirm the validity and robustness of the proposed theoretical analysis. **The revised portion is shown below.**

#### (Page 4) Sec. II

...Fig. 18a shows that  $c$  does not decrease the amplitude but changes the positions of the peak and the foot. Besides, we present the designed phase shifts feasible set in the complex plane relative to the ideal unit circle under variations in  $a$ ,  $b$ , and  $c$ . Based on Fig. 18b increasing  $a$  shifts and squeezes the set with a non-monotonic area that shrinks for large  $a$ . Fig. 18c shows increasing  $b$  roughly scales it up, enlarging the area and approaching the unit circle, and Fig. 18d reveals  $c$  mainly causes a global rotation with nearly constant area. Thus, in order to mimic the real pixel device, choosing a suitable  $b$  is of great significance. We then have a proposition as follows...

#### (Pages 13-14) Sec. III, A-D

...From Fig. 19a, it can be observed that the empirical PDF of  $\phi_m$  distributed over  $[-\pi, \pi]$ , this aligns with our assumption in the last step of (3). Fig. 27a shows that decreasing the area of the pixel (i.e.,  $d_x d_y$ ) would diminish the SE. Besides, the upper bound of the SE would approach the simulated results, i.e., (47) becomes  $SE_L = SE_L^{\text{Upper}} > SE = SE^{\text{Upper}} > SE_U = SE_U^{\text{Upper}}$ . This is because the area and the center point of the pixel can be regarded the same when  $d_x = d_y \leq \frac{\lambda}{4}$ , and shows the correctness of Theorem 1. Although  $\phi_m \sim \mathcal{UF}[-\pi, \pi]$ , Fig. 19c shows  $\Gamma$  exhibits a U-shaped distribution. This is caused by the

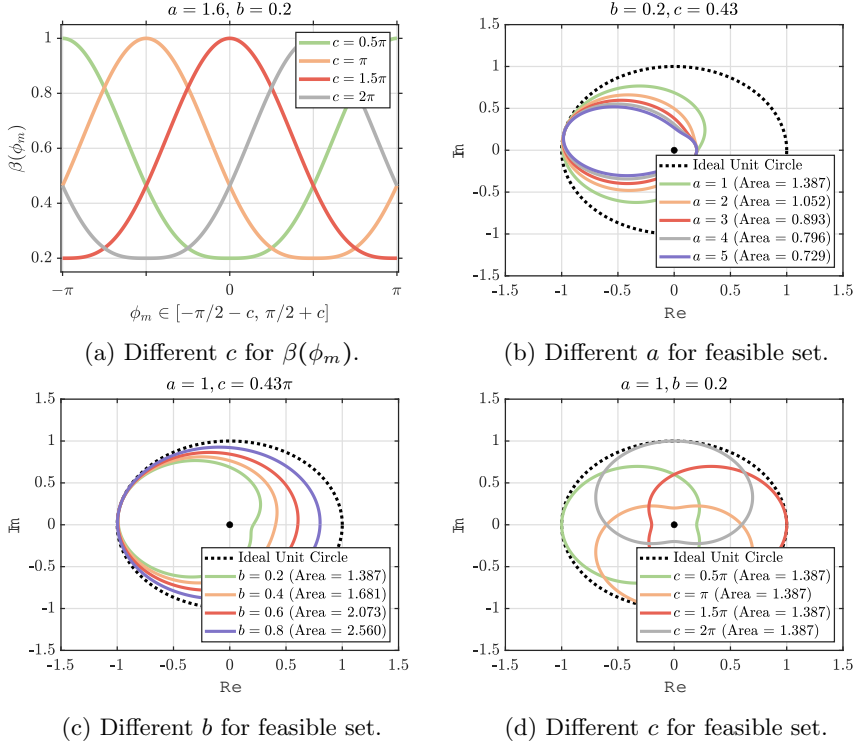


Figure 18: Approximated PDA model validations and phase shift feasible set plots. Electrical parameters are from [18].

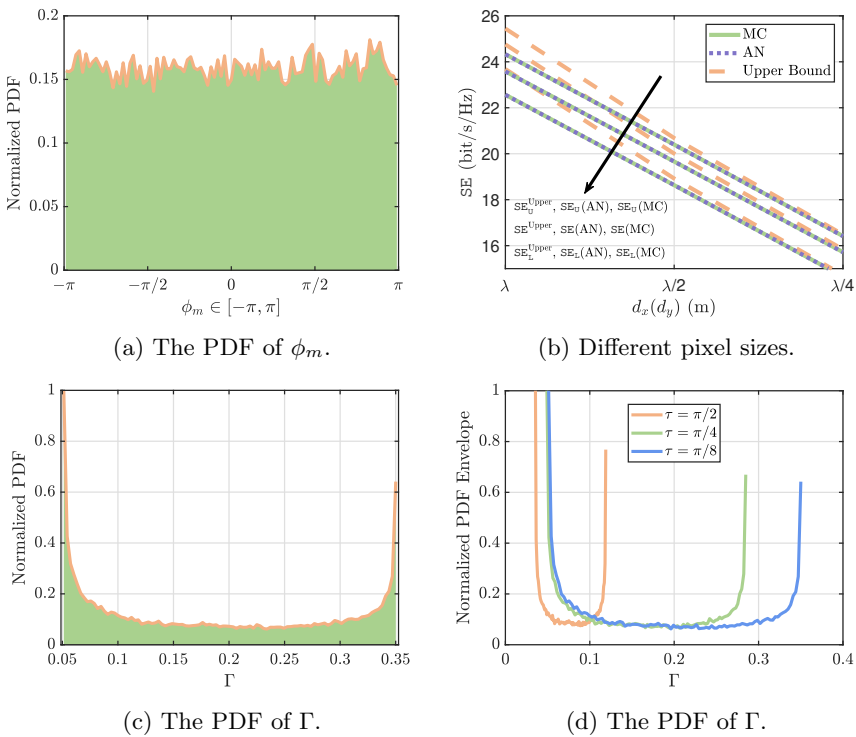


Figure 19: System performance when the RIS is fixed.

nonlinear feature of the PDA. Fig. 19d illustrates the PDFs for different values of  $\tau$ , showing broader distributions and reduced peaks as  $\tau$  increases, while a similar trend can be observed when  $\kappa$  decreases...

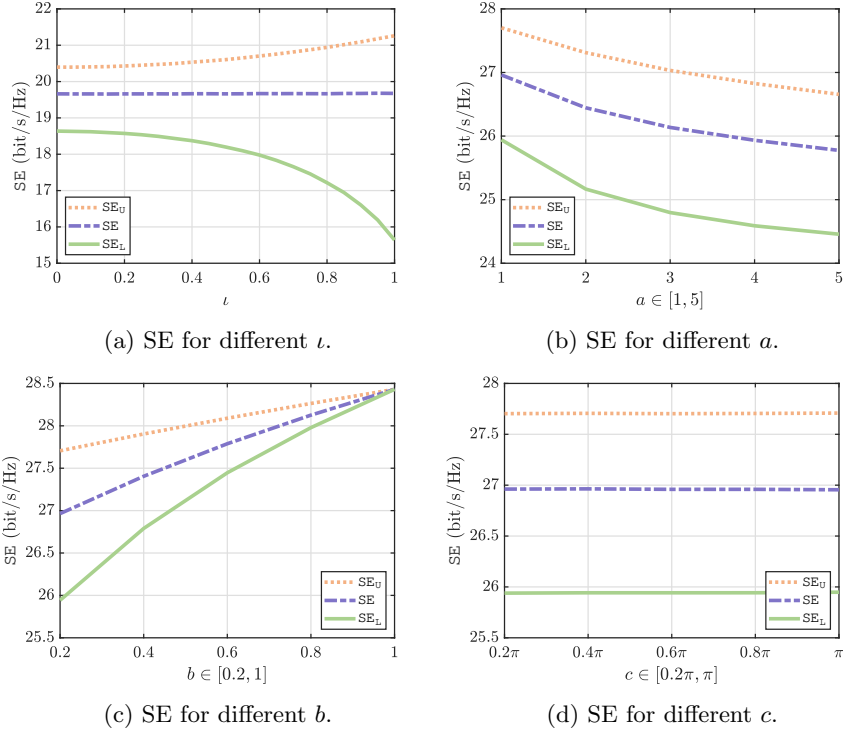


Figure 20: SE performance for different parameters.

...Fig. 20 illustrates the SE for different  $\iota$ ,  $a$ ,  $b$ , and  $c$ . As expected, when  $\phi_m = \phi_L$ , SE decreases as  $\iota$  increases, consistent with Figs. (4) and (13). Moreover, SE increases with smaller  $a$  and decreases with larger  $b$ . In contrast,  $c$  has negligible impact on SE because it only shifts the PDA curve. This result is in good agreement with...

...Fig. 21 visualizes  $\phi_m$  and  $\Gamma$  by using heatmap. With  $\tau = \pi/8$  and  $\kappa = 2, 5, 8$ , we can see that  $\phi_m$  is approximately uniform over  $[-\pi, \pi]$ . Besides, as  $\kappa$  decreases, phase concentration decreases and both the peak and span of high  $\Gamma$  regions shrink, with weak sensitivity to  $M$ . These trends align with the SE improving as noise decreases...

...Fig. 27b verifies the correctness of Theorem 1 in Sec. IV, as MC and AN results match well. Moreover, SE first decreases and then increases, as the RIS performs worst when it is deployed in the middle of the AP and the user [26]. Fig. 22b shows heatmap of  $\phi_m$  when  $x_{\text{RIS}} = 8$ . Compare to Fig. 21a with  $x_{\text{RIS}} = 0$ , although the overall periodic pattern remains similar, slight displacements in the central region and phase gradient occur, indicating that the horizontal shift of the RIS introduces spatial variations in the phase distribution. Figs. 22c and 22d demonstrate that the statistical distributions of  $\phi_m$  and  $\Gamma$  are independent of the RIS's position, as the curves for different  $x_{\text{RIS}}$  are nearly identical...

...Next, we consider the RIS center is set to  $[0, 10, z_{\text{RIS}}]^T$  m with  $z_{\text{RIS}} \in [-20, 10]$  m, and the Doppler effect is neglected. Fig. 23a illustrates that as  $z_{\text{RIS}}$  increases, the SE first rises due to the reduced propagation distance, but then falls as the projected aperture diminishes to nearly zero. However, as shown in Fig. 23b, without the projected aperture, the SE is simply inversely proportional to the distance between the transmitter and receiver. Besides,  $\text{SE}_{\text{Prop.3.10}}$  is smallest, as expected...

...Figs. 24 show the feasible sets for designed RIS phases in the complex plane and their corresponding areas for the different propositions in Sec. III. As expected, greater uncertainties lead to smaller feasible set areas. Moreover, the areas and  $\iota$  are inversely related. This suggests that RIS designs should be optimized to minimize noise coupling. Specifically, during the initial deployment of the RIS (i.e.,  $\iota = 1$ ), an optimization constraint can be formulated to ensure that the optimal phase remains close to the phase boundaries. However, after prolonged operation (i.e.,  $\iota = 0$ ), this constraint should be reformulated to keep the optimal phase near the middle of the phase range...

---

**Comment 1.6:** There are multiple issues with non-standard formula formatting and inconsistent no-

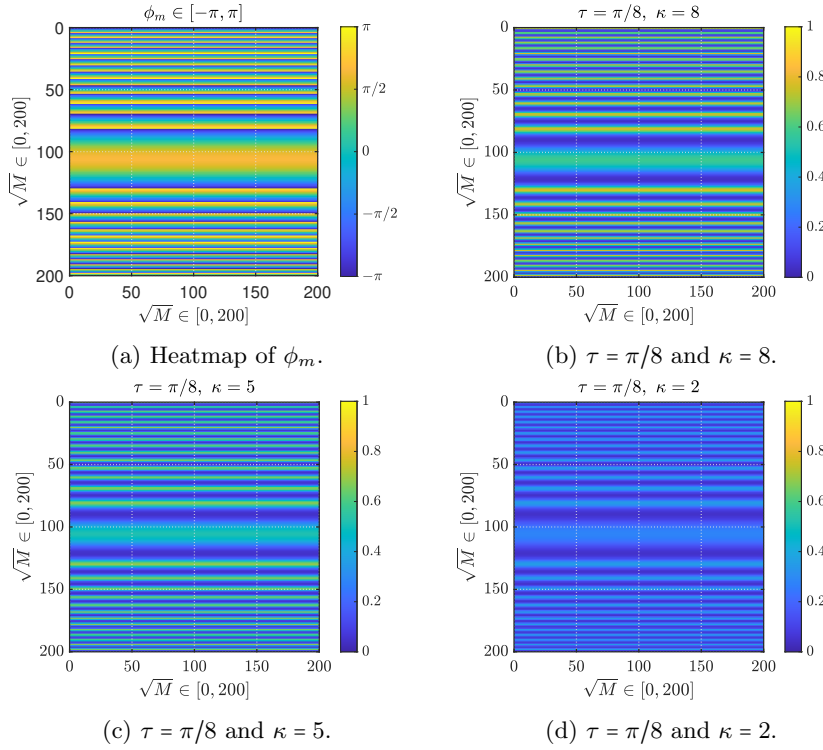


Figure 21: Heatmaps of  $\phi$  and  $\Gamma$  when the RIS is fixed.

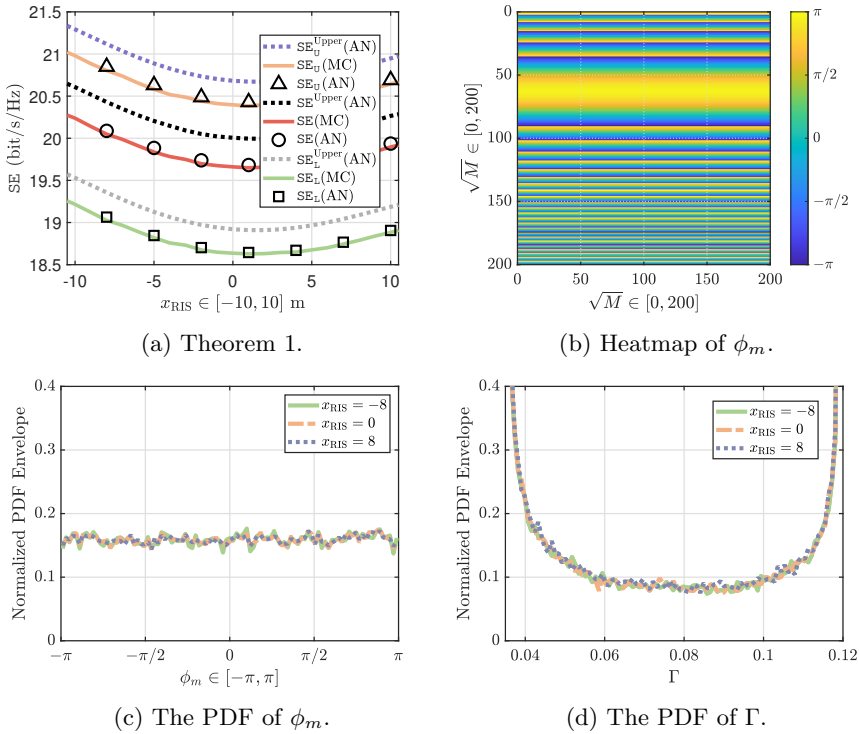


Figure 22: System performance for the RIS  $x$ -axis movement.

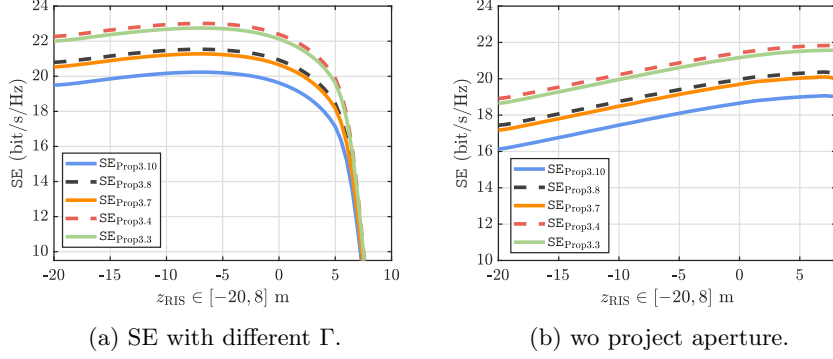


Figure 23: System performance for the RIS  $z$ -axis movement.

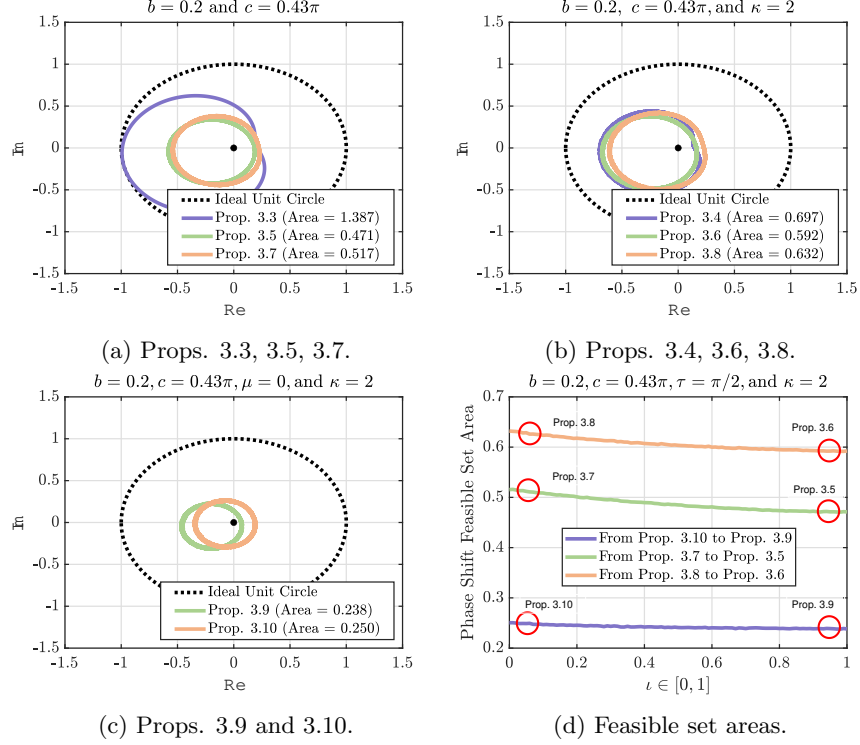


Figure 24: Feasible set and areas.

tation throughout the manuscript. Please check the formula formatting and notation consistency across the entire manuscript. Additionally, explanations of variable substitutions in key derivation steps in the appendix are insufficient, making the derivation process less clear.

**Response 1.6:** We sincerely thank the reviewer for this valuable comment. In the revision, we have carefully checked all formulas and mathematical symbols throughout the manuscript to ensure standard formatting and consistent notation. In particular, we have unified the representations of key parameters across the main text and the appendix. Moreover, the variable substitutions and intermediate derivation steps in the appendix have been clarified in greater detail; specifically, explicit explanations have been added for the transformations used in the equations of Appendix E. These improvements enhance the readability and transparency of the theoretical derivations and enable the reader to follow the mathematical logic more easily. **Please kindly check the revised manuscript.**

## To Reviewer 2

---

**Comment 2.1:** This paper has investigated an important mutual coupling loss in the RIS-aided system. Four distinct pixel reflection models, each involving several types of PEs, have been introduced, and the respective approximate upper bounds for the PL have been derived. Besides, a new upper bound of the SE was proposed for the RIS-aided system with the mutual coupling loss. This work is solid and well-written.

**Response 2.1:** We sincerely thank the reviewer for the positive and encouraging comment on our work.

---

**Comment 2.2:** In (8),  $\phi_m$  is omitted when calculating the summation. However, in the near-field,  $\phi_m$  may not be the same. Does this omission impact the results?

**Response 2.2:** We sincerely thank the reviewer for this valuable comment. We agree that this is an important issue closely related to the core analysis of our work. Therefore, in order to investigate the impact of noise, we first assume  $\phi_1 = \phi_2 = \dots = \phi_M$  in Props. 3.3 - 3.10. Second, in a more general setting, the total power radiated by the RIS is given by (8) in the manuscript as

$$\begin{aligned}
P_{\text{RIS}} &= \left| \sum_{m=1}^M \sqrt{P_{\text{AP} \rightarrow m}} \underbrace{\beta(\phi_m + \bar{\Delta}_m)}_{\text{PE}} \underbrace{\exp(-j\Delta_m)}_{\text{PE}} \right|^2 \\
&\stackrel{(i)}{=} P_{\text{AP} \rightarrow 1} \left| \sum_{m=1}^M \beta(\phi_m + \bar{\Delta}_m) \exp(-j\Delta_m) \right|^2 \\
&= M^2 P_{\text{AP} \rightarrow 1} \left| \frac{1}{M} \sum_{m=1}^M \beta(\phi_m + \bar{\Delta}_m) \exp(-j\Delta_m) \right|^2 \\
&\xrightarrow{M \rightarrow \infty} M^2 P_{\text{AP} \rightarrow 1} \underbrace{\left| \mathbb{E}\{\beta(\phi + \bar{\Delta}) \exp(-j\Delta)\} \right|^2}_{\substack{\text{Square Law} \\ \text{Remaining Power } \Gamma \in (0,1)}}, \tag{3}
\end{aligned}$$

where  $\exp(-j\Delta)$  does not contain  $\phi_m$  because the designed  $\phi_m$  and the phase of the cascaded channel cancel each other out. However, the  $\phi_m$  in  $\beta(\phi_m + \bar{\Delta}_m)$  cannot be omitted, and each  $\phi_m$  differs under the NF scenario. To address this issue, we first assume that  $\phi_m$  follows a uniform distribution  $\mathcal{U}[-\pi/2 - c, \pi/2 + c]$ . This assumption is reasonable, especially when the number of pixels is sufficiently large. Then, by leveraging the extended Glivenko–Cantelli theorem<sup>1</sup>, we obtain the last step in (3) as  $M \rightarrow \infty$ . Finally, we perform simulations to verify this result. We state that when  $\iota = 0$ , as  $M$  increases from 1 to 200, MC result  $\Gamma_M = \left| \frac{1}{M} \sum_{m=1}^M \beta(\phi_m + \bar{\Delta}_m) \exp(-j\Delta_m) \right|^2$  converges asymptotically to AN limit  $\Gamma_\infty = \left| \mathbb{E}\{\beta(\phi + \bar{\Delta}) \exp(-j\Delta)\} \right|^2$ . When  $\iota = 1$ , we need a larger  $M$  to achieve convergence. **The revised portion is shown below.**

(Page 5) Sec. III

...where (i) is obtained when the pixels are all with the same transmit power  $P_{\text{AP} \rightarrow 1} = P_{\text{AP} \rightarrow 2} = \dots = P_{\text{AP} \rightarrow M}$ , respectively. As the number of reflecting elements  $M$  becomes sufficiently large, the phase shift

<sup>1</sup>When the empirical distribution of a deterministic sequence converges weakly to a probability distribution, the average of any function over that sequence converges to the expectation of the corresponding random variable.

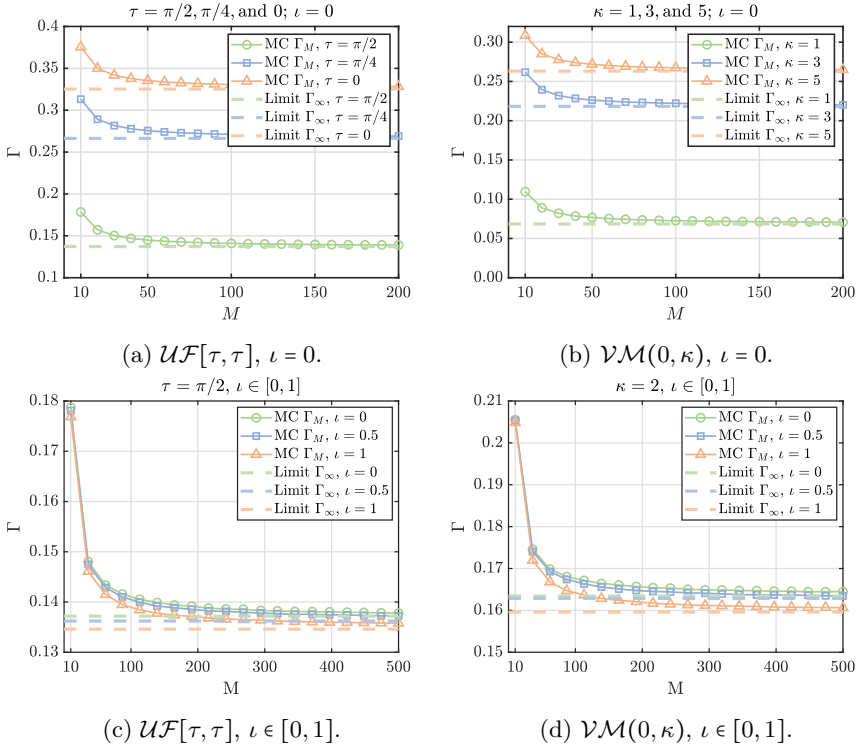


Figure 25: Validation of (8),  $\nu = 0$  or 1.

set  $\{\phi_m\}_{m=1}^M$ , which is designed to be densely and uniformly distributed over the interval  $[-\pi/2-c, \pi/2+c]$ , form a sequence whose empirical distribution function converges to that of a continuous  $\mathcal{UF}$  distribution over  $[-\pi/2-c, \pi/2+c]$ . By considering an extension of the *Glivenko–Cantelli theorem* [30], for the bounded continuous functions  $\beta(\phi + \bar{\Delta}) \exp(-j\Delta)$ , the final step of (3) is obtained..

**Comment 2.3:** In (33), an upper bound is derived using Jensen's inequality. Could  $L$  be proved as a strict lower bound?

**Response 2.3:** We sincerely thank the reviewer for this valuable comment. We confirm that  $L$  indeed serves as a strict lower bound. Recall that we have

$$\begin{aligned} L &= \mathbb{E} \left\{ \left| \sum_{m=1}^M g_m \beta(\phi_L + \Delta_m) \exp(-j(\phi_m + \Delta_m)) h_m \right|^2 \right\} \\ &\approx \left( \sum_{m=1}^M A_{AP \rightarrow m} \sqrt{\Gamma_{(.)}(\phi_L)} A_{m \rightarrow User} \right)^2 \\ &= \Gamma_{(.)}(\phi_L) \left( \sum_{m=1}^M A_{AP \rightarrow m} A_{m \rightarrow User} \right)^2, \end{aligned} \quad (4)$$

where  $\phi_L = -\pi/2 + c$ . That means  $\beta(\phi_L) = (1-b) \cdot \left( \frac{\sin(-\pi/2+c-c)+1}{2} \right)^a + b = b$ , thus the amplitude approaches its minimum. Similarly, we have  $\beta(\phi_U) = (1-b) \cdot \left( \frac{\sin(\pi/2+c-c)+1}{2} \right)^a + b = 1$ . It is important to note that the PSE part, i.e.,  $\exp(\phi_m + j\Delta)$  is always with the  $\phi_m$ , so  $L$  and  $U$  only relay on the amplitude  $\beta(\cdot)$ . Therefore,  $L$  and  $U$  all belongs to Case I in Table 1, i.e.,  $\beta \cdot \exp(-j\Delta)$ , and  $\beta = b$  and 1, respectively. Therefore,  $L$  is a strict lower bound. **The revised portion is shown below.**

#### (Page 4), Sec. II and (Pages 13-14), Sec. V, A, B

...It shows the relationship between phase shift  $\phi_m \in [-\pi/2 - c, \pi/2 + c]$  and reflected amplitude  $\beta(\phi_m) \in [b, 1]$ . When  $\phi_m = \pi/2 + c$ , the amplitude  $\beta(\phi_m)$  is maximized to 1. This is because the reflective currents are out-of-phase with the pixel currents. However, when  $\phi_m = -\pi/2 + c$ , the amplitude is minimized to  $b$  since the dielectric and metallic losses increase...

**Proposition 2** (Lower and upper bounds of the ideal PDA): *When the pixel hardware and the phase shift are both noiseless, the lower and upper bounds of  $\beta(\phi_m)$  in [6] are given by*

$$b \stackrel{(i)}{\leq} \beta(\phi_m) \Big|_{a>1} \stackrel{(ii)}{\leq} \beta(\phi_m) \Big|_{a=1} \stackrel{(iii)}{\leq} 1. \quad (5)$$

*Proof:* First, when  $\phi_m = \phi_L$ , equality holds in (i). Similarly, (ii) holds with equality when  $\beta(\phi_m)$  attains its minimum (maximum), respectively. Moreover, since  $\sin(\phi_m - c) \in [0, 1]$  and  $b \in [0, 1]$ , it is straightforward to verify (iii). This completes the proof.  $\blacksquare$

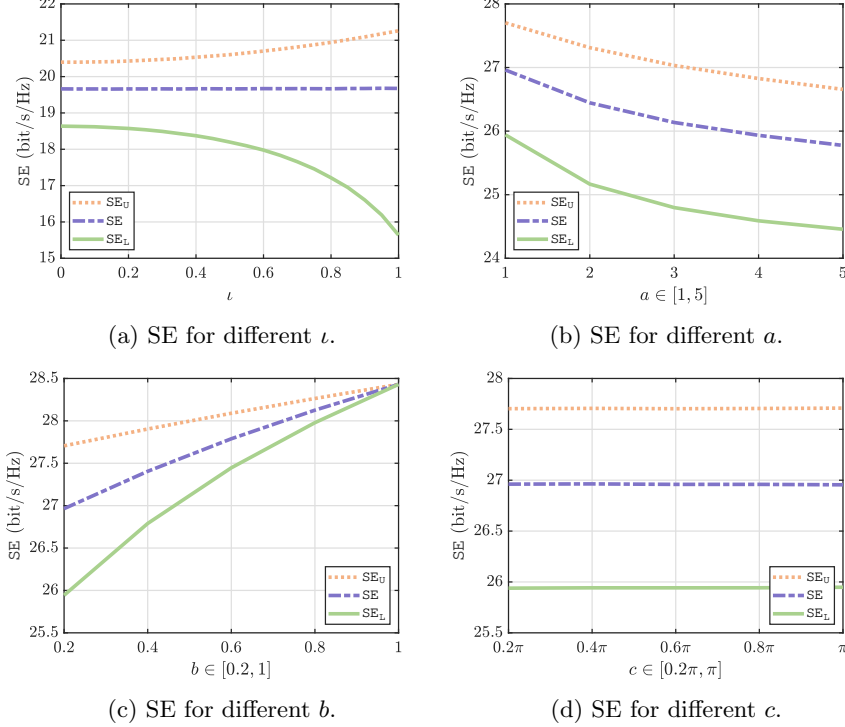


Figure 26: SE performance for different parameters.

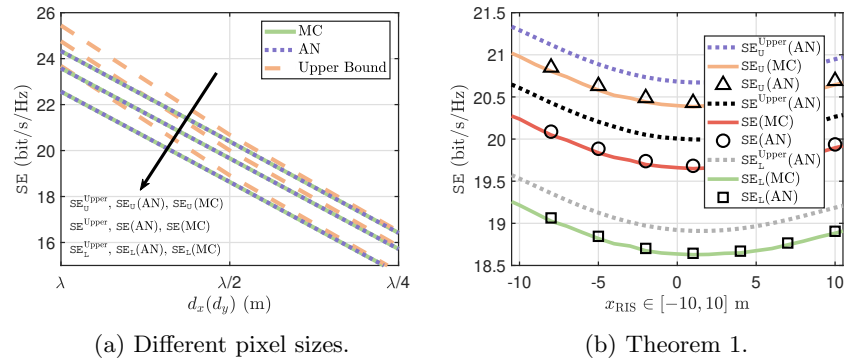


Figure 27: SE performance.

**Comment 2.4:** Section III contains intensive derivations. What insights can be drawn from Section III?

**Response 2.4:** We sincerely thank the reviewer for this valuable comment. Sec. III establishes a unified theoretical framework to quantify how phase errors jointly affect the PDAs and PSEs in near-field RISs. The section defines the RP metric and, by employing the extended Glivenko–Cantelli theorem, proves the asymptotic convergence of reflected power as the number of pixels increases.

Furthermore, four reflection cases I to IV are derived to represent different combinations of amplitude and phase disturbances, with analytical upper bounds obtained via Taylor expansion  $\mathcal{UF}$  and  $\mathcal{VM}$  distributed errors. The results indicate that the coupling between PDA and PSE significantly impacts RIS performance, i.e., independent errors may outperform fully correlated ones near phase minima, while the opposite occurs near maxima. These findings explain the performance gap between ideal and practical RISs and provide the theoretical foundation for the SE analysis in Sec. IV.

Finally, based on these results, we further reveal that during the initial deployment of the RIS (i.e.,  $\iota = 1$ ), an optimization constraint can be formulated to ensure that the optimal phase remains close to the phase boundaries. However, after prolonged operation (i.e.,  $\iota = 0$ ), this constraint should be reformulated to keep the optimal phase near the middle of the phase range. **The revised portion is shown below.**

#### (Page 8, Remark I)

*...Remark I (In Fig. 29a, why  $\phi_m = \pi/2$  has the smallest error when  $\phi_m$  is close to  $\pi/2$ ?): In Fig. 29a, the error is smallest when  $\phi_m$  is close to  $\pi/2$ , because the PDA is less sensitive to the PE near this point. Specifically, in the PDA model, at  $\phi_m \approx \pi/2$ , the derivative  $\partial\beta(\phi_m)/\partial\phi_m$  is small, resulting in milder changes in it when adding  $\delta_m$ . Thus, the Taylor expansion approximation based on small  $\tau$  is more accurate, with reduced impact from higher-order terms, leading to the minimal error...*

#### (Page 9, Remark II)

*...Remark II (If  $\phi_m$  approaches to 0, why  $\Gamma$  decreases when  $\iota$  increases?): As observed in Figs. 13a and 13a, the RP  $\Gamma$  decreases as  $\phi_m$  approaches 0. For instance,  $\Gamma$  is slightly lower at  $\phi_m \approx 0$  than at  $\phi_m \approx \pi/4$ . This is because when  $\phi_m \approx 0$ , the system operates near the linear region of the phase response function  $\beta(\cdot)$ . As the correlation coefficient  $\iota$  increases from 0 toward 1, the amplitude and phase noise become increasingly coupled. This coupling induces a negative covariance between the amplitude and the phase. We provide a strict proof of  $\Gamma(0)|_{\iota=0} > \Gamma(0)|_{\iota=1}$  in Appendix B. Fig. 3 verify this remark through MC simulations of vector field distributions under  $\mathcal{UF}$  and  $\mathcal{VM}$  RVs, respectively. In particular, when  $\phi_m = 0$ , length of the synthesized vector  $|\mathbf{P}_{\iota=1}| < |\mathbf{P}_{\iota=0}|$  and the inequality is reversed when  $\phi_m = \pi/2$ ...*

---

**Comment 2.5:** In Section IV, can the results be adapted to a multi-user scenario?

**Response 2.5:** We sincerely thank the reviewer for this valuable comment. The analytical framework in Section IV can indeed be extended to a multi-user scenario. Specifically, the derived expressions for the PDA and power scaling laws remain valid when multiple users are served, as each user experiences an individual cascaded channel through the RIS. In this case, the system performance can be evaluated by integrating user-specific channel responses into the total received power expression and considering possible inter-user interference. For simplicity and clarity, our current work focuses on the single-user case to highlight the key insights of phase-error coupling. Nevertheless, extending the analysis to a multi-user setting is straightforward and will be an important direction for our future work.

Moreover, the findings in Section III provide direct guidance for extending the analysis to multi-user scenarios. The revealed coupling characteristics between the PDA and PSE can be used to model the phase and amplitude distortions caused by users located at different spatial positions. In particular, since users at different locations experience different incidence angles and phase centers, independent errors may outperform correlated ones near phase minima. Therefore, the phase optimization strategy can be adaptively adjusted according to each user's position and operating region. These insights offer valuable guidelines for coordinated RIS control in multi-user environments, helping to mitigate spatial coupling losses and enhance overall system efficiency. **The revised portion is shown below.**

#### (Page 15, Sec. VI)

*...Future work will focus on RIS phase optimization considering the coupling between the PDA and PE. For active RISs, where the PDA is more complex [40], it is also important to investigate imperfections in the relationship between the PDA and the PE within each active pixel. Another research direction is how to quantitatively characterize the phase and amplitude of an RIS pixel as it transitions from fully coupled to fully independent, which, based on known results, is closely related to hardware aging that*

occurs over time during operation [17]. Furthermore, we will extend these studies to multi-user scenarios to analyze the impact of the coupling on beamforming and interference control...

## To Reviewer 3

---

**Comment 3.1:** *The authors considered four different pixel reflection models and derived their corresponding upper bounds on the power loss. The bounds for the spectral efficiency are also derived. In general, the paper's structure is clear and easy to follow; the theoretical derivations are also solid..*

**Response 3.1:** We sincerely thank the reviewer for the positive and encouraging comment on our work.

---

**Comment 3.2:** *Explain the relationship and difference between the terms 'PE' and 'PSE' in Sec. I-A.*

**Response 3.2:** We sincerely thank the reviewer for this valuable comment. We agree that clarifying the relationship and distinction between “phase errors (PEs)” and “phase shift with errors (PSEs)” will help improve the clarity of the paper. Specifically, the abbreviation PE stands for “phase error,” which not only appears in the phase component but may also be transferred to the amplitude. In particular, as shown in Case III of Table 1, we propose the reflection model as  $\beta(\phi + \bar{\Delta}) \cdot \exp(-j\Delta)$ . In this model, the PEs are represented by  $\bar{\Delta}$  and  $\Delta$ , which can be identical, i.i.d., or partially correlated. In addition,  $\exp(-j\Delta)$  represents the phase shift with error (PSE), corresponding to the phase component of the proposed reflection model that incorporates the PE. Moreover,  $\beta(\phi + \bar{\Delta})$  denotes the phase-dependent amplitudes (PDAs) with the PE. **The revised portion is shown below.**

(Pages 1-2, Sec. I)

...Moreover, in practical scenarios, phase errors (PEs) within the RIS cannot be overlooked [10]. Previous studies [10]–[16] primarily focused on phase shift with errors (PSEs), represented as  $\exp(-j(\phi + \Delta))$  where  $\phi$  denotes an RIS pixel phase shift,  $\Delta$  represents a PE random variable (RV) follows specific distributions...

...Beyond the aforementioned noises exist in the PSE  $\exp(-j\Delta)$ , however, the actual pixel reflection coefficient exhibits its own *phase-dependent amplitudes (PDAs)*...

Model	Works	Reflection Coefficient Description	Approximated Model
Perfect	[3-9], [26-28]	...	$1 \cdot \exp(-j\phi)$
Case I	[10-16], [29]	...	$\beta \cdot \exp(-j\Delta)$
Case II	[17-20]	...	$\beta(\phi) \cdot \exp(-j\Delta)$
Case III	This paper	...	$\beta(\phi + \bar{\Delta}) \cdot \exp(-j\Delta)$
Case IV	This paper	...	$\beta(\phi + \bar{\Delta} + \bar{\Theta}) \cdot \exp(-j(\Delta + \Theta))$

Table 1: Comparison between this paper and its related works. Note  $\beta(\cdot) \in (0, 1]$  and  $\phi$  is the designed pixel phase shift.  $\Delta$ ,  $\bar{\Delta}$ ,  $\Theta$  and  $\bar{\Theta}$  all denote PE RVs,  $\bar{\Delta} = \iota\Delta + \sqrt{1 - \iota^2}\bar{\Delta}$ , where  $\iota \in [0, 1]$  and  $\bar{\Delta}$  is i.i.d. with  $\Delta$ .  $\Theta$  and  $\bar{\Theta}$  are defined analogously.

---

**Comment 3.3:** *Table I is not clear enough. Provide a more detailed explanation for the approximated models and the notations within in Sec. I-B.*

**Response 3.3:** We sincerely thank the reviewer for this valuable comment. **The revised portion is shown below.**

(Page 2, Sec. I, B)

...Thus, from a practical perspective, the PDA may also exist the PE. To this end, in this paper, we consider three regimes: (i) perfect transfer of the PE from the PSE to the PDA, i.e.,  $\iota = 1$  in Cases III and IV in Table I; (ii) fully random pixel imperfections that induce i.i.d. noise at the PDA, i.e.,  $\iota = 0$  in Cases III and IV in Table I; and (iii) intermediate correlation levels with  $\iota \in (0, 1)$ . In practice, the pixel hardware failure [14-17] progressively shifts the system from (i) toward (ii). Specifically, differential degradation of RIS components (e.g., varactor diodes) desynchronizes the errors between the PSE and the PDA, thereby increasing their *statistical independence*. Consequently, as the RIS behavior approaches an i.i.d. noise model, the correlation coefficient  $\iota$  decreases over time and approaches 0, reflecting the emergence of random, decoupled uncertainties driven by hardware degradations [17]...

**Comment 3.4:** Do not use interrogative sentences in Sec. I-B, which is confusing.

**Response 3.4:** We sincerely thank the reviewer for this valuable comment. We have already revised Sec. I, B to make sure there is no interrogative sentences. **The revised portion is shown below.**

**(Page 2, Sec. I, B)**

...Thus, from a practical perspective, the PDA may also exist the PE. To this end, in this paper, we consider three regimes: (i) perfect transfer of the PE from the PSE to the PDA, i.e.,  $\iota = 1$  in Cases III and IV in Table I; (ii) fully random pixel imperfections that induce i.i.d. noise at the PDA, i.e.,  $\iota = 0$  in Cases III and IV in Table I; and (iii) intermediate correlation levels with  $\iota \in (0, 1)$ . In practice, the pixel hardware failure [14-17] progressively shifts the system from (i) toward (ii). Specifically, differential degradation of RIS components (e.g., varactor diodes) desynchronizes the errors between the PSE and the PDA, thereby increasing their *statistical independence*. Consequently, as the RIS behavior approaches an i.i.d. noise model, the correlation coefficient  $\iota$  decreases over time and approaches 0, reflecting the emergence of random, decoupled uncertainties driven by hardware degradations [17]...

...It is noteworthy that the omission of the above issues may be pivotal in accounting for the disparity between theoretical analyses and hardware validations [22-25]. Besides, different from the existing pixel reflection models (i.e., Perfect, Cases I and II in Table I), a practical model that explicitly captures  $\mathcal{UF}$  and/or  $\mathcal{VM}$  uncertainties in the PSE and/or the PDA is essential for future performance analysis and algorithm design in the NF RIS-assisted system. Therefore, the focus of this work is to determine *how the PSE and the PDA, with the PE in particular, jointly affect the RIS system performance*. The contributions are summarized as follows...

---

**Comment 3.5:** The Propositions in Sec. III and the Theorem in Sec. IV should be referred to and analyses in the text. Provide insights for them.

**Response 3.5:** We sincerely thank the reviewer for this valuable comment. We agree that clearer analysis and discussion of the Propositions in Section III and the Theorem in Section IV will improve the paper's logical flow and clarity.

Sec. III establishes a unified framework to quantify the joint effect of PEs on PDAs and PSEs, and defines the RP metric. Based on the extended Glivenko–Cantelli theorem, it proves the asymptotic convergence of reflected power with increasing pixel numbers. Through Taylor expansion with  $\mathcal{UF}$  and  $\mathcal{VM}$  distributed errors, four reflection cases (I–IV) and their analytical upper bounds are derived. The results show that the PDA–PSE coupling significantly affects RIS performance: i.i.d. errors outperform correlated ones near phase minima, while the opposite occurs near maxima. These findings reveal the gap between ideal and practical RISs and provide the theoretical basis for the SE analysis in Sec. IV.

In Sec. IV, building on the Friis transmission formula and the proposed reflection framework, we establish a general NF LoS channel model that incorporates the coupling between the PDA and the PSE. A closed-form SE expression is further derived using the CauchyBunyakovskySchwarz inequality and Riemann sums. The analysis shows that the derived upper bound becomes tighter with smaller pixel areas, effectively capturing the influence of PDA–PSE coupling on NF RIS channel behavior and SE limits. **The revised portion is shown below.**

**(Page 8, Remark I)**

**...Remark I** (In Fig. 29a, why  $\phi_m = \pi/2$  has the smallest error when  $\phi_m$  is close to  $\pi/2$ ?): *In Fig. 29a, the error is smallest when  $\phi_m$  is close to  $\pi/2$ , because the PDA is less sensitive to the PE near this point. Specifically, in the PDA model, at  $\phi_m \approx \pi/2$ , the derivative  $\partial\beta(\phi_m)/\partial\phi_m$  is small, resulting in milder changes in it when adding  $\delta_m$ . Thus, the Taylor expansion approximation based on small  $\tau$  is more accurate, with reduced impact from higher-order terms, leading to the minimal error...*

**(Page 9, Remark II)**

**...Remark II** (If  $\phi_m$  approaches to 0, why  $\Gamma$  decreases when  $\iota$  increases?): *As observed in Figs. 13a and 13a, the RP  $\Gamma$  decreases as  $\phi_m$  approaches 0. For instance,  $\Gamma$  is slightly lower at  $\phi_m \approx 0$  than at  $\phi_m \approx \pi/4$ . This is because when  $\phi_m \approx 0$ , the system operates near the linear region of the phase response function  $\beta(\cdot)$ . As the correlation coefficient  $\iota$  increases from 0 toward 1, the amplitude and phase noise become increasingly coupled. This coupling induces a negative covariance between the amplitude and the phase. We provide a strict proof of  $\Gamma(0)|_{\iota=0} > \Gamma(0)|_{\iota=1}$  in Appendix ???. Fig. 3 verify this remark through MC simulations of vector field distributions under  $\mathcal{UF}$  and  $\mathcal{VM}$  RVs, respectively. In particular, when  $\phi_m = 0$ , length of the synthesized vector  $|\mathbf{P}_{\iota=1}| < |\mathbf{P}_{\iota=0}|$  and the inequality is reversed when  $\phi_m = \pi/2$ ...*

(Page 11, Remark III)

**...Remark III:** Note that for the RIS with  $M$  pixels,  $\Gamma_m$  generally differ because each scatterer exhibits distinct characteristics. Consequently, the term  $\beta(\phi_m + \Delta_m)$  of  $h$  in (32) cannot be factored outside the summation, and a closed-form expression for  $\Gamma_m$  is generally unavailable. However, based on the last step of (8), when the number of pixels is sufficiently large (e.g., larger than 200), the RP obtained in the previous section can be used to evaluate the SE. Accordingly, in the next section, we derive the SE expression together with its lower and upper bounds...

---

**Comment 3.6:** The Remarks are not necessary and cause visual confusion. Just put them in the regular text.

**Response 3.6:** We sincerely thank the reviewer for this valuable comment. We have already removed all unnecessary remarks. Please kindly check pages 4 - 10.

---

**Comment 3.7:** Explain how the derived bounds are supposed to be utilized in practical IRS-assisted systems? Are they effective as objective functions when considering IRS phase shift optimization problems?

**Response 3.7:** We sincerely thank the reviewer for this valuable comment. We agree that clarifying the practical use of the derived bounds is important. The derived analytical bounds have strong theoretical and practical relevance for RIS-assisted systems. They provide closed-form upper and lower limits for performance under PEs, PDAs, and PSEs, enabling fast performance estimation and parameter tuning without intensive simulations. In optimization problems, these bounds can serve as differentiable surrogate objectives or constraints, supporting robust and low-complexity phase design. Particularly under limited phase resolution or known error statistics, the upper bound facilitates convex approximation or gradient-based optimization toward near-optimal solutions. When errors are small, the bounds remain tight and accurate for algorithm benchmarking; under larger or uncertain errors, they serve as conservative yet meaningful design references. **The revised portion is shown below.**

(Page 14, Sec. V, D)

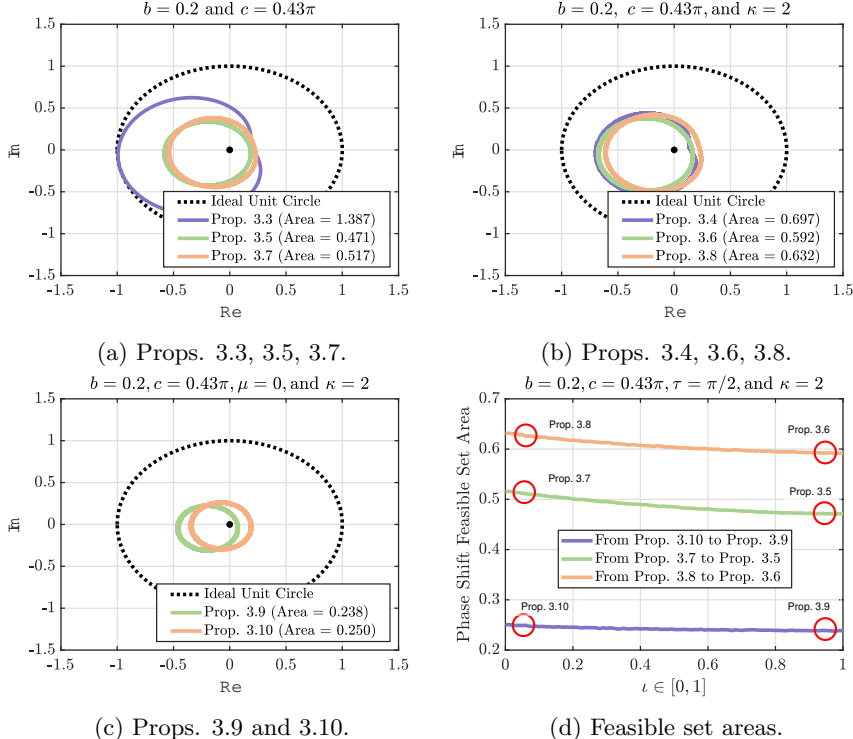


Figure 28: Feasible set and areas.

...Figs. 24 show the feasible sets for designed RIS phases in the complex plane and their corresponding areas for the different propositions in Sec. III. As expected, greater uncertainties lead to smaller feasible set areas. Moreover, the areas and  $\tau$  are inversely related. This suggests that RIS designs should be optimized to minimize noise coupling. Specifically, during the initial deployment of the RIS (i.e.,  $\tau = 1$ ),

an optimization constraint can be formulated to ensure that the optimal phase remains close to the phase boundaries. However, after prolonged operation (i.e.,  $\iota = 0$ ), this constraint should be reformulated to keep the optimal phase near the middle of the phase range...

**Comment 3.8:** When validating the propositions in Sec. III, how did the authors generate the Monte Carlo values for upper bounds? Since the derived functions are called bounds, they should be deterministic; why are there MC values?

**Response 3.8:** We sincerely thank the reviewer for this valuable comment. The upper bound is obtained when  $\phi_m = \phi_U = \pi/2 + c$ . For example, consider  $\Gamma_{(3.3)} \leq \Gamma_{(3.3)}^* < \Gamma_{(3.3)}^*(\phi_U)$  in Sec. II, we have  $\Gamma_{(3.3)} = |\mathbb{E}\{\beta(\phi_m) \exp(-j\delta_m)\}|^2$ ,  $\Gamma_{(3.3)}^* = |\mathbb{E}\{\bar{\beta}(\phi_m) \exp(-j\delta_m)\}|^2 = \zeta \left(1 - \frac{1}{3}\tau^2 + \frac{2}{45}\tau^4 - \frac{1}{360}\tau^6 + \frac{1}{14400}\tau^8\right) + \mathcal{O}(\tau^{10})$  and  $\zeta = \frac{(1-b)^2}{4} \sin^2(\phi_m - c) + \frac{(1-b^2)}{2} \sin(\phi_m - c) + \frac{(1+b)^2}{4}$ . We can obtain that when  $\phi_m = \phi_U = \pi/2 + c$ ,  $\zeta = \frac{(1-b)^2}{4} + \frac{(1-b^2)}{2} + \frac{(1+b)^2}{4} = 1$ . Thus,  $\Gamma_{(3.3)}^*(\phi_U) = \left(1 - \frac{1}{3}\tau^2 + \frac{2}{45}\tau^4 - \frac{1}{360}\tau^6 + \frac{1}{14400}\tau^8\right)$ .

We use an MATLAB program to show how to generate the MC values for upper bounds. We still consider Prop. 3.3, it shows that

```

1 a=1;b=0.2;c=0.43*pi;phi_m=pi/2;
2 beta_m=(1-b)*((sin(phi_m-c)+1)/2)^a+b;
3 x=linspace(0,pi/2,10);
4 realization_number=1e6;
5 delta_m=zeros(length(x),realization_number);
6 for i=1:length(x)
7 delta_m(i,:)=random('Uniform',-x(i),x(i),1,realization_number);
8 end
9 Gamma_33_star_MC=abs(mean(beta_m*exp(-1i*delta_m),2)).^2';
10 Gamma_33_star_AN=((1-b)^2/4*(sin(phi_m-c))^2+(1-b^2)/2*sin(phi_m-c)+...
11 (1+b)^2/4)*(1-(1/3)*x.^2+(2/45)*x.^4-(1/360)*x.^6+(1/14400)*x.^8);
12 a=2;
13 beta_mn_2=(1-b)*((sin(phi_m-c)+1)/2)^a+b;
14 Gamma_33_MC_a_2=abs(mean(beta_mn_2*exp(-1i*delta_m),2)).^2';
15 a=3;
16 beta_mn_3=(1-b)*((sin(phi_m-c)+1)/2)^a+b;
17 Gamma_33_MC_a_3=abs(mean(beta_mn_3*exp(-1i*delta_m),2)).^2';
18 phi_U=pi/2+c;
19 a=1;
20 beta_phi_U=(1-b)*((sin(phi_U-c)+1)/2)^a+b;
21 Gamma_33_star_phi_U_MC=abs(mean(beta_phi_U*exp(-1i*delta_m),2)).^2';
22 Gamma_33_star_phi_U_AN=(1-(1/3)*x.^2+(2/45)*x.^4-(1/360)*x.^6+(1/14400)*x.^8);

```

Please note that the last two lines generate the AN and MC results of the  $\Gamma_{(3.3)}^*(\phi_U)$ , respectively. In particular, the MC here means we let  $\phi_m = \phi_U = \pi/2 + c$ , and compute  $\Gamma_{(3.3)}^* = |\mathbb{E}\{\bar{\beta}(\phi_U) \exp(-j\delta_m)\}|^2$ , and the AN means we use  $\Gamma_{(3.3)}^*(\phi_U) = \left(1 - \frac{1}{3}\tau^2 + \frac{2}{45}\tau^4 - \frac{1}{360}\tau^6 + \frac{1}{14400}\tau^8\right)$  directly. Besides, we have added the AN result for Props. 3.3-3.10. Please check in Sec. III (pages 4 - 10) of the revised manuscript.

**Comment 3.9:** It is noticed that the MC results do not match the AN values well when  $x$  is near 1.5 in Fig. 7 (a). Please explain the phenomenon. Is this kind of mismatch acceptable? Please verify.

**Response 3.9:** We sincerely thank the reviewer for this valuable comment. The mismatch is caused by insufficient expansion terms. We have already fixed this issue, now the AN and MC result matches well. Besides, we also added the error term to the AN expression and plotted it in the figure. For example, for Prop. 3.5, we have

...**Proposition 3.5** ( $\beta(\phi_m + \delta_m) \exp(-j\delta_m)$ ,  $\iota = 1$ ): When the  $m$ -th PDA is  $\beta(\phi_m + \delta_m)$ , and the PDA and the PSE all contain  $\delta_m \sim \mathcal{U}\mathcal{F}[-\tau, \tau]$  where  $\tau \in [0, \pi/2]$ , then the upper bound of the RP  $\Gamma$  in (16) can be obtained as

$$\Gamma_{(3.5)} \leq \Gamma_{(3.5)}^* = (\eta_1 + \eta_2)^2 + \eta_3 < \Gamma_{(3.5)}^*(\phi_U), \quad (6)$$

where  $\Gamma_{(3.5)} = \left| \mathbb{E}\{\beta(\phi_m + \delta_m) \exp(-j\delta_m)\} \right|^2$ ,  $\Gamma_{(3.5)}^* = \left| \mathbb{E}\{\bar{\beta}(\phi_m + \delta_m) \exp(-j\delta_m)\} \right|^2$ ,  $\eta_1 = \frac{(1-b)}{2} \sin(\phi_m - c)(1 - \frac{1}{3}\tau^2 + \frac{1}{15}\tau^4 - \frac{2}{315}\tau^6) + \mathcal{O}(\tau^8)$ ,  $\eta_2 = \frac{1+b}{2}(1 - \frac{1}{6}\tau^2 + \frac{1}{120}\tau^4 - \frac{1}{5040}\tau^6) + \mathcal{O}(\tau^8)$ ,  $\eta_3 = \frac{(1-b)^2}{4}(\frac{1}{3}\tau^2 - \frac{1}{15}\tau^4 + \frac{2}{315}\tau^6)^2 \cos^2(\phi_m - c) + \mathcal{O}(\tau^{12})$ ,  $\Gamma_{(3.5)}^{\text{Error}} = |\Gamma_{(3.5)}^{\text{MC}} - \Gamma_{(3.5)}^{\text{AN}}| \sim \mathcal{O}(\tau^8)$ .  $\Gamma_{(3.5)}^*(\phi_U) = (\eta_1 / \sin(\phi_m - c) + \eta_2)^2 \dots$

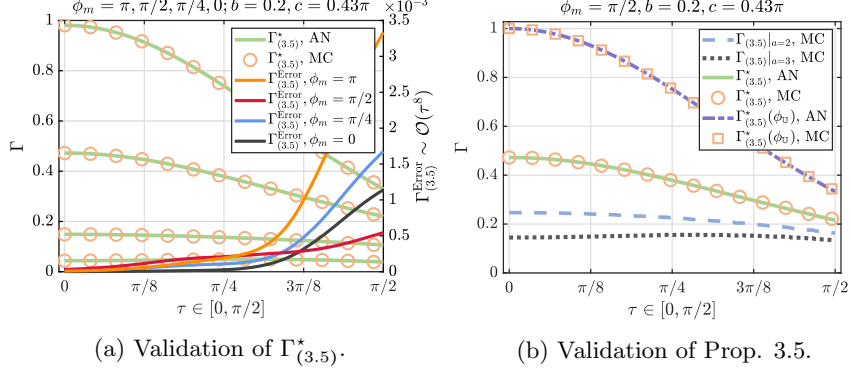


Figure 29: Validation of Prop. 3.5.

We did the same revision to other propositions. Please check in Sec. III (pages 4 - 10) of the revised manuscript.